cmgh
CELLULAR AND MOLECULAR GASTROENTEROLOGY AND HEPATOLOGY

ORIGINAL RESEARCH

Hepatocyte Deubiquitinating Enzyme OTUD5 Deficiency Is a Key Aggravator for Metabolic Dysfunction-Associated Steatohepatitis by Disturbing Mitochondrial Homeostasis

Jingjing Dai,[1,*] Liren Zhang,[2,*] Ruizhi Zhang,[2,*] Jing Ge,[3,*] Feifan Yao,[2,*] Suiqing Zhou,[2,*] Jiali Xu,[4,*] Kai Yu,[2] Jing Xu,[5] Longfeng Jiang,[1] Ke Jin,[1] Xinzheng Dai,[2] Jun Li,[1] and Qing Li[2]

[1]Department of Infectious Diseases, The First Affiliated Hospital of Nanjing Medical University, Nanjing, Jiangsu Province, China; [2]Hepatobiliary Center, The First Affiliated Hospital of Nanjing Medical University; Key Laboratory of Liver Transplantation, Chinese Academy of Medical Sciences; NHC Key Laboratory of Living Donor Liver Transplantation (Nanjing Medical University), Nanjing, Jiangsu Province, China; [3]Department of Endocrinology, Jiangsu Province Hospital of Chinese Medicine, Affiliated Hospital of Nanjing University of Chinese Medicine, Nanjing, Jiangsu Province, China; [4]Department of Anesthesiology, Jinling Hospital, Affiliated Hospital of Medical School, Nanjing University, Nanjing, Jiangsu Province, China; and [5]Department of Oncology, The First Affiliated Hospital of Nanjing Medical University, Nanjing, Jiangsu Province, China

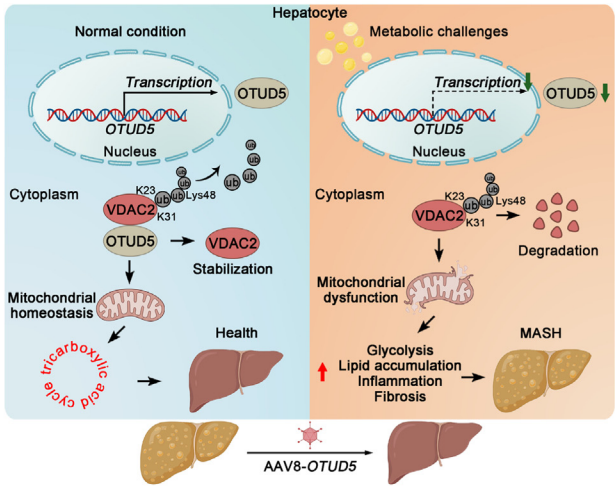

SUMMARY

Metabolic dysfunction–associated steatohepatitis (MASH) is a common chronic liver disease worldwide. We found that OTUD5 may ameliorate MASH progression via VDAC2-maintained mitochondrial homeostasis. OTUD5 may be a promising target for effectively treating MASH.

BACKGROUND & AIMS: Metabolic dysfunction–associated steatohepatitis (MASH) is a common chronic liver disease worldwide. No effective pharmacologic therapies for MASH have been developed; to develop such promising drugs, the underlying mechanisms regulating MASH need to be elucidated. Here, we aimed to determine the role of ovarian tumor domain-containing protein 5 (OTUD5) in MASH progression and identify a specific mechanism.

METHODS: The expression levels of OTUD subfamily under palmitic acid/oleic acid (PAOA) stimulation were screened. OTUD5 expression was assessed in human liver tissues without steatosis, those with simple steatosis, and those with MASH. MASH models were developed in hepatocyte-specific *Otud5*-knockout mice that were fed high-fat high-cholesterol and high-fat high-cholesterol plus high-fructose/sucrose diet for 16 weeks.

RESULTS: The expression of OTUD5 was down-regulated in fatty liver and was negatively related to the progression of MASH. Lipid accumulation and inflammation were exacerbated by *Otud5* knockdown but attenuated by *Otud5* overexpression under PAOA treatment. Hepatocyte-specific *Otud5* deletion markedly exacerbated steatosis, inflammation, and fibrosis in the livers of 2 MASH mouse models. We identified voltage-dependent anion channel 2 (VDAC2) as an OTUD5-interacting partner; OTUD5 cleaved the K48-linked polyubiquitin chains from VDAC2, and it inhibited subsequent proteasomal degradation. The anabolic effects of OTUD5 knockdown on PAOA-induced lipid accumulation were effectively reversed by VDAC2 overexpression in primary hepatocytes. Metabolomic results revealed that VDAC2 is required for OTUD5-mediated protection against hepatic steatosis by maintaining mitochondrial function.

CONCLUSIONS: OTUD5 may ameliorate MASH progression via VDAC2-maintained mitochondrial homeostasis. Targeting OTUD5 may be a viable MASH-treatment strategy. *(Cell Mol Gastroenterol Hepatol 2024;17:399–421; https://doi.org/10.1016/j.jcmgh.2023.11.014)*

Keywords: Ovarian Tumor Domain-Containing Protein; Ubiquitination; Metabolism; Mitochondrial Function.

With prominent changes in diet and lifestyle, nonalcoholic fatty liver disease, now referred to as metabolic dysfunction–associated steatotic liver disease (MASLD), has become the most prevalent metabolic liver disorder, and it manifests as excessive hepatic lipid accumulation.[1–5] The prevalence of MASLD is increasing, and it currently affects approximately 25% of adults worldwide.[6–10] Metabolic dysfunction–associated steatohepatitis (MASH), which is the progressive stage of MASLD, is characterized by severe hepatic steatosis, inflammation, and fibrosis. MASH can eventually result in cirrhosis or hepatocellular carcinoma.[11–15] Owing to its complexity and heterogeneous pathogenesis, no valid clinically applicable pharmacologic therapy is currently available.[16–20] Hence, a detailed understanding of the molecular mechanisms underlying MASLD is urgently needed to develop promising therapeutic targets and strategies.

Ubiquitination is an invertible biological process that is concurrently regulated by E3 ubiquitin ligases and deubiquitinases (DUBs).[21–25] Compared with E3 ubiquitin ligases, which have been widely investigated in MASLD, DUBs are relatively underappreciated by researchers.[26–28] DUBs principally cleave ubiquitin chains from ubiquitin-conjugated proteins to inhibit ubiquitin-mediated degradation and to maintain the stability of their target proteins. Currently, more than 100 human DUBs have been recognized and classified into 7 families: ubiquitin-specific proteases (USPs), ovarian tumor-associated proteases (OTUs), Machado-Joseph disease protein proteases, ubiquitin C-terminal hydrolase family (UCHs), monocyte chemotactic protein-induced proteins, JAMM/MPN domain-associated metallopeptidases, and motif-interacting with ubiquitin containing proteases.[29,30] As the second largest human family of DUBs, 16 active OTU family DUBs in humans are classified into 4 subfamilies: the OTU domain-containing ubiquitin aldehyde-binding proteins (Otubains) subfamily (OTUB1, OTUB2), the ovarian tumor domain-containing protein (OTUD) subfamily (OTUD1, OTUD2, OTUD3, OTUD4, OTUD5, OTUD6A, OTUD6B, and ALG13), the A20-like subfamily (A20, OTUD7A, OTUD7B, TRABID, and VCPIP), and the OTU DUB with linear linkage specificity. Compared with other subfamilies, the biological function of OTUDs is relatively underappreciated, especially in hepatic disorders. In particular, the involvement of OTUDs in MASLD progression remains to be explored.[31,32]

Herein, we screened the expression profiles of the OTUD subfamily in human and primary mouse hepatocytes under palmitic acid/oleic acid (PAOA) stimulation and focused on OTUD5. OTUD5 was originally identified as a negative regulator of type I interferon, and it functions in innate immunity.[33] Recently, its importance in acquired immunity has also been uncovered.[34] Many studies have revealed the role of OTUD5 in the development and progression of immune disorders and inflammation.[35] Moreover, OTUD5 has also been investigated in various cancers to determine its oncogenic or anti-oncogenic effects depending on the substrates. OTUD5 acts as a tumor inhibitor in non-small cell lung cancer and cervical cancer.[36,37] However, OTUD5 promotes carcinogenesis in triple-negative breast cancer and bladder cancer.[38,39] Hence, the specific function of OTUD5 in different cancers needs to be analyzed on a case-to-case basis. Herein, we found that the expression of OTUD5 is decreased in fatty liver and is negatively related to MASLD progression. OTUD5 knockout/knockdown markedly contributed to hepatic steatosis, inflammation, and fibrosis under metabolic stress in both in vivo and in vitro models. Moreover, voltage-dependent anion channel 2 (VDAC2) is required for OTUD5-mediated protection against hepatic steatosis by maintaining mitochondrial function. Crucially, our findings suggest that OTUD5 may be a promising target for effectively treating MASLD.

Results

Expression Level of OTUD5 Decreased in Fatty Liver and Was Negatively Related to MASLD Progression

To comprehensively investigate the role of OTUD subfamily in MASLD progression, we first investigated their expression profiles in human and primary mouse hepatocytes under PAOA stimulation. Quantitative real-time polymerase chain reaction (qRT-PCR) analysis revealed that *OTUD5* mRNA achieved the highest fold-change consistently in both human and primary mouse hepatocytes, indicating that OTUD5 might have a unique role in modulating MASLD progression (Figure 1*A* and *B*). Therefore, we determined the expression of OTUD5 in normal human livers without steatosis and in those with simple steatosis or MASH. Hepatic *OTUD5* mRNA levels were significantly lower in livers with simple steatosis or MASH than

*Authors share co-first authorship.

Abbreviations used in this paper: **AAV, adeno-associated virus; ALT, alanine aminotransferase; AST, aspartate aminotransferase; BSA, bovine serum albumin; DUBs, deubiquitinases; HFHC, high-fat high-cholesterol; HFF, high-fat high-cholesterol plus high-fructose/sucrose; IP, immunoprecipitation; MASH, metabolic dysfunction–associated steatohepatitis; MASLD, metabolic dysfunction–associated steatotic liver disease; NAS, nonalcoholic fatty liver disease activity score; NC, normal chow; OTUBs, OTU domain-containing ubiquitin aldehyde-binding proteins; OTUD5, ovarian tumor domain-containing protein 5; OTUs, ovarian tumor-associated proteases; PAOA, palmitic acid/oleic acid; qRT-PCR, quantitative real-time polymerase chain reaction; TC, total cholesterol; TCA, tricarboxylic acid; TG, triglyceride; UCHs, ubiquitin C-terminal hydrolase family; USPs, ubiquitin-specific proteases; VDAC2, voltage-dependent anion channel 2.**

Most current article

2352-345X
https://doi.org/10.1016/j.jcmgh.2023.11.014

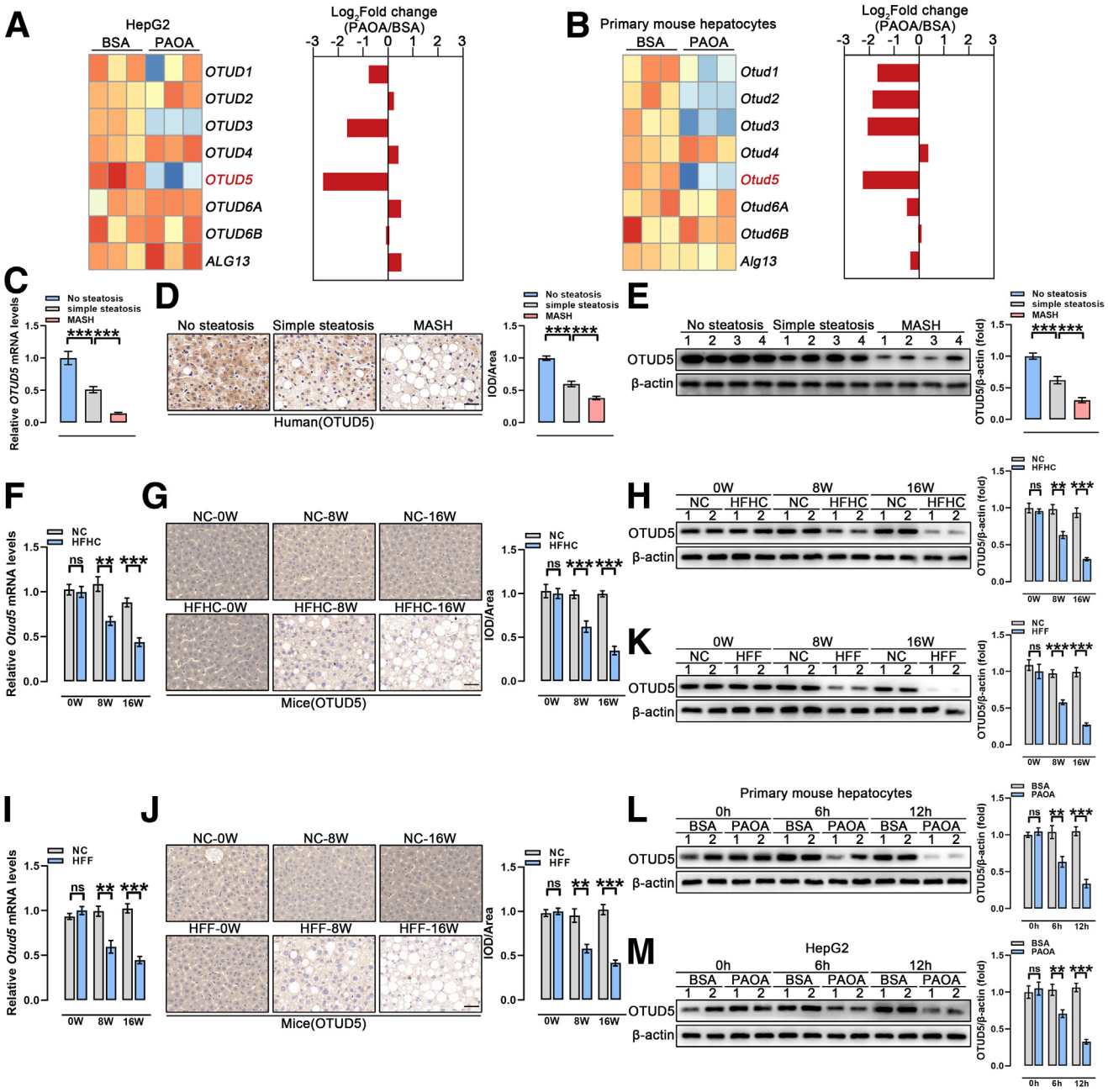

Figure 1. OTUD5 expression is down-regulated in fatty liver. (*A*) qRT-PCR analysis showing expression of OTUD subfamily in HepG2 cells under PAOA stimulation. (*B*) qRT-PCR analysis showing expression of OTUD subfamily in primary mouse hepatocytes under PAOA stimulation. (*C*) Relative *OTUD5* mRNA levels in normal human livers without steatosis (n = 20) and those with simple steatosis (n = 20) or MASH (n = 20). (*D*) Representative immunohistochemical staining images and quantification of OTUD5 expression in normal human livers (n = 20) and those with simple steatosis (n = 20) or MASH (n = 20). Scale bar: 50 μm. (*E*) Representative Western blot analysis and quantification of OTUD5 expression in normal human livers (n = 20) and those with simple steatosis (n = 20) or MASH (n = 20). (*F*) Relative *Otud5* mRNA levels in livers of C57BL/6J mice with NC diet or HFHC diet for indicated weeks. n = 6 mice/group. (*G*) Representative immunohistochemical staining images and quantification of OTUD5 expression in livers of C57BL/6J mice with NC diet or HFHC diet for indicated weeks. Scale bar: 50 μm. n = 6 mice/group. (*H*) Representative Western blots analysis and quantification of OTUD5 protein levels in livers of C57BL/6J mice with NC diet or HFHC diet for indicated weeks. n = 6 mice/group. (*I*) Relative *Otud5* mRNA levels in livers of C57BL/6J mice with NC diet or HFF diet for indicated weeks. n = 6 mice/group. (*J*) Representative immunohistochemical staining images and quantification of OTUD5 expression in livers of C57BL/6J mice with NC diet or HFF diet for indicated weeks. Scale bar: 50 μm. n = 6 mice/group. (*K*) Representative Western blots analysis and quantification of OTUD5 protein levels in livers of C57BL/6J mice with NC diet or HFF diet for indicated weeks. n = 6 mice/group. (*L*) OTUD5 protein levels in primary hepatocytes stimulated with BSA or PAOA. (*M*) OTUD5 protein levels in HepG2 cells stimulated with BSA or PAOA. For all panels, data are presented as mean ± standard error of the mean, and n represents biologically independent repeats. *P* values were calculated using two-tailed unpaired Student *t* test. $^{**}P < .01$; $^{***}P < 0.001$; ns, not significant.

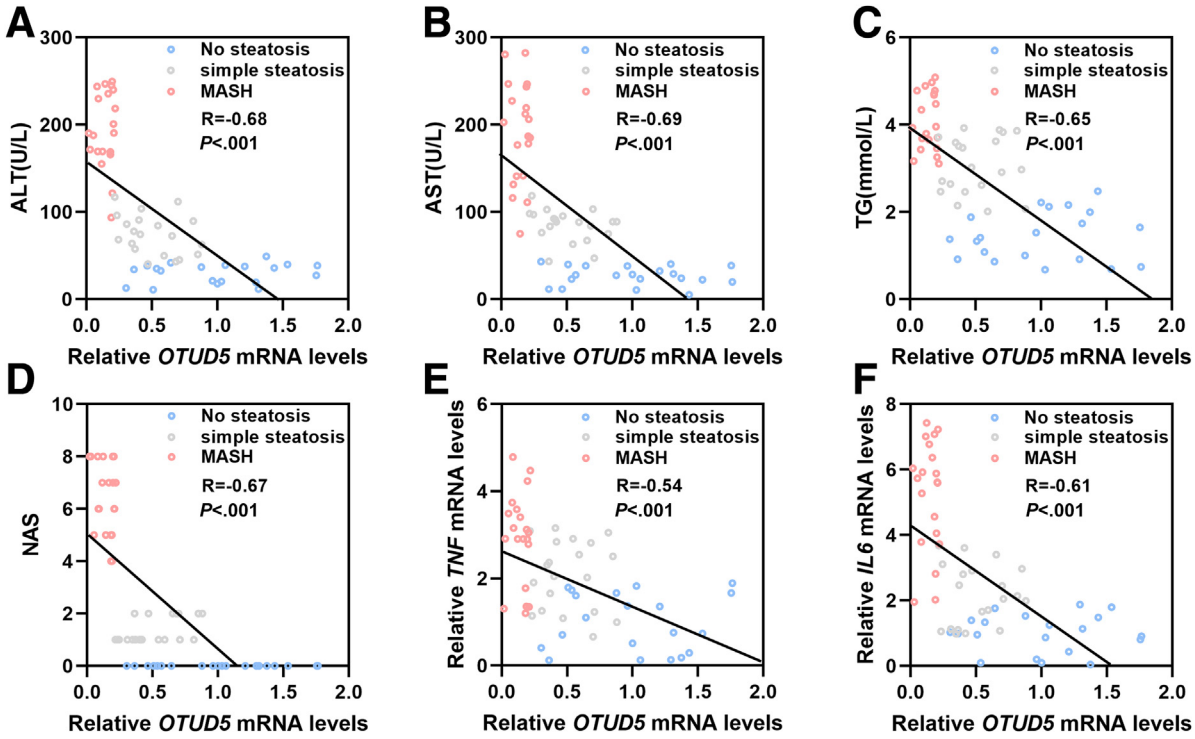

Figure 2. OTUD5 expression is negatively related to MASLD progression. (*A–F*) Pearson analysis of correlation between *OTUD5* mRNA levels and serum ALT levels (*A*), serum AST levels (*B*), serum TG levels (*C*), NAS levels (*D*), mRNA levels of *TNF* (*E*), and *IL6* mRNA levels (*F*) in normal human livers (n = 20) and those with simple steatosis (n = 20) or MASH (n = 20). For all panels, n represents biologically independent repeats. *P* values were calculated by Pearson correlation analysis.

in normal human livers. Moreover, human livers with MASH had lower *OTUD5* mRNA levels than those with simple steatosis (Figure 1*C*). In line with the alteration of *OTUD5* mRNA levels, its protein expression level was lower in human livers with simple steatosis or with MASH than that in normal human livers. The livers with MASH had significantly lower OTUD5 protein levels than the livers with simple steatosis, as indicated by immunohistochemical staining and Western blot analysis (Figure 1*D* and *E*). Consistent with our findings in human individuals, OTUD5 expression levels of both mRNA and proteins were evidently decreased in mouse livers with high-fat high-cholesterol (HFHC) or high-fat/high-cholesterol plus high fructose/sucrose (HFF) diets compared with their littermates that were fed a normal chow (NC) diet (Figure 1*F–K*). Similarly, OTUD5 expression level gradually decreased over time in isolated primary mouse hepatocytes and HepG2 cells in the presence of PAOA compared with bovine serum albumin (BSA)-treated control cells (Figure 1*L* and *M*).

We further validated the clinical relevance of *OTUD5* expression levels and the severity of liver disease in patients with MASH. Using Pearson correlation analysis, we determined that serum alanine aminotransferase (ALT), aspartate aminotransferase (AST), triglyceride (TG), nonalcoholic fatty liver activity score (NAS), and mRNA expression levels of *TNF* and *IL6* were negatively correlated with *OTUD5* mRNA levels (Figure 2*A–F*). We classified the patients with MASH into 2 groups based on the median value of *OTUD5* mRNA levels, a group with high expression level of *OTUD5* (10/20, $OTUD5^{high}$ group) and a group with low expression level of *OTUD5* (10/20, $OTUD5^{low}$ group). The severity of inflammation, fibrosis, and liver lipogenesis was reduced, whereas β-oxidation was enhanced in the $OTUD5^{high}$ group compared with that in the $OTUD5^{low}$ group (Figure 3*A–C*). Moreover, the expression levels of *Col1a1* and *Fasn* decreased, whereas expression level of *Cpt1a* increased in the $OTUD5^{high}$ group compared with those in the $OTUD5^{low}$ group (Figure 3*D*).

OTUD5 Ameliorated PAOA-Induced Lipid Accumulation and Inflammation in Hepatocytes

To investigate the influence of OTUD5 expression on lipid accumulation and inflammation in hepatocytes, primary hepatocytes were isolated and infected with adenovirus vector-mediated *OTUD5*-knockdown (Adsh*OTUD5*) or *OTUD5*-overexpression plasmid (Ad*OTUD5*-Flag). qRT-PCR analysis and Western blotting confirmed *OTUD5* knockdown in Adsh*OTUD5*-infected primary hepatocytes and *OTUD5* overexpression in Ad*OTUD5*-infected primary hepatocytes (Figure 4*A* and *B*). The transfection efficiency of Adsh*OTUD5#3* was satisfactory for subsequent experiments. As indicated by Nile red staining, Oil Red O staining, and TG concentrations, no visible difference in hepatocyte lipid accumulation was observed after *OTUD5* expression level alteration under BSA-treated conditions. Nevertheless, PAOA-induced hepatocyte lipid accumulation in Adsh*OTUD5*-infected primary hepatocytes was significantly aggravated compared with that in the AdshRNA group. Adsh*OTUD5*-infected primary hepatocytes were detected at higher concentrations of TG. In contrast, *OTUD5* overexpression in

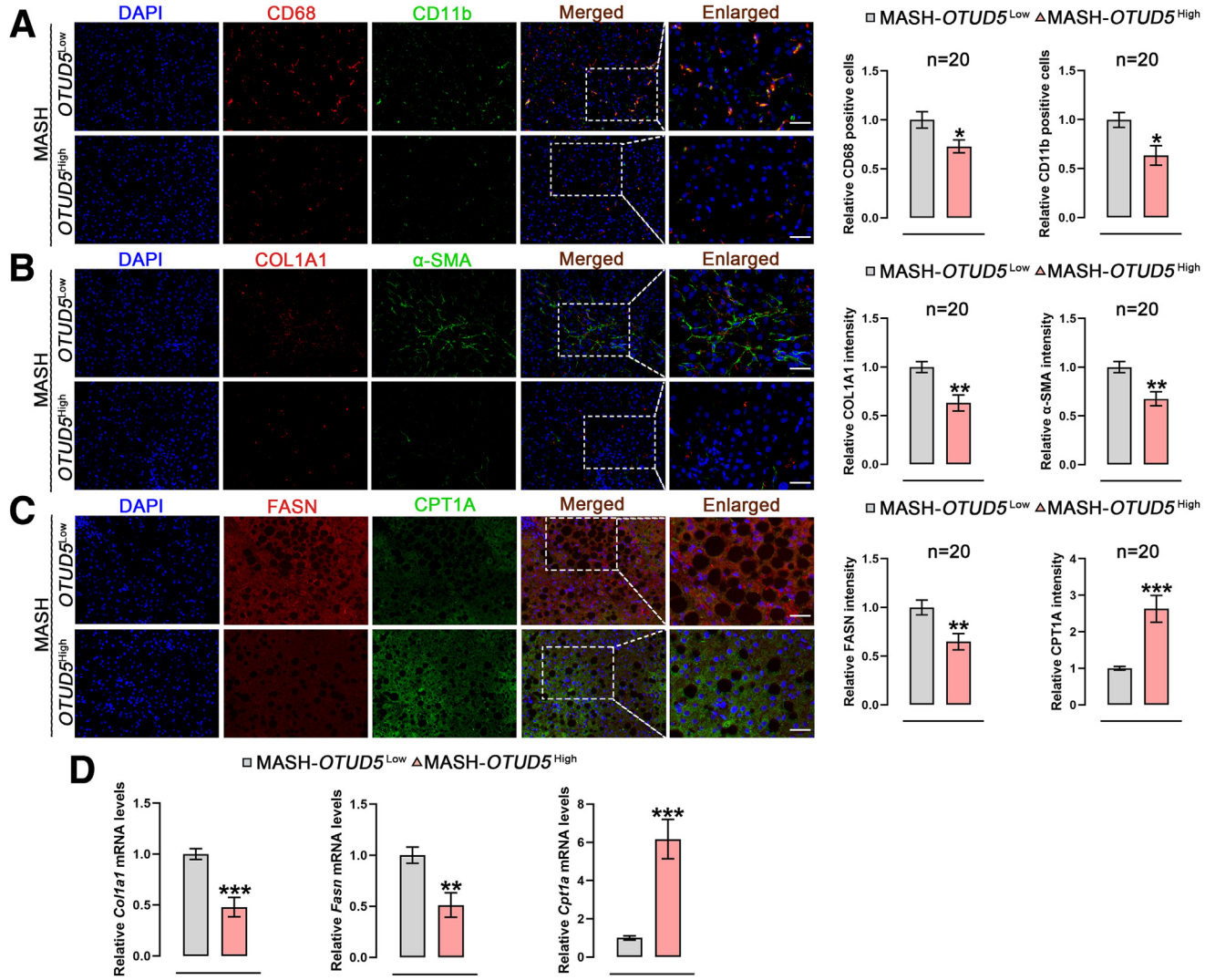

Figure 3. OTUD5 expression is negatively related to MASLD progression. (*A*) Left: representative immunofluorescence staining showing CD68 (*red*) and CD11b (*green*) in sections of *OTUD5*^{low} and *OTUD5*^{high} MASH livers. Scale bar: 50 μm. Right: quantification of CD68^{+} and CD11b^{+} cells. n = 10 patients/group. (*B*) Left: representative immunofluorescence staining showing COL1A1 (*red*) and α-SMA (*green*) in sections of *OTUD5*^{low} and *OTUD5*^{high} MASH livers. Scale bar: 50 μm. Right: quantification of COL1A1 and α-SMA fluorescence intensities. n = 10 patients/group. (*C*) Left: representative immunofluorescence staining showing FASN (*red*) and CPT1A (*green*) in sections of *OTUD5*^{low} and *OTUD5*^{high} MASH livers. Scale bar: 50 μm. Right: quantification of FASN and CPT1A fluorescence intensities. n = 10 patients/group. (*D*) Relative mRNA expression levels of *Col1a1*, *Fasn*, and *Cpt1a* of *OTUD5*^{low} and *OTUD5*^{high} MASH livers. For all panels, data are presented as mean ± standard error of the mean, and n represents biologically independent repeats. *P* values were calculated using two-tailed unpaired Student *t* test. **P* < .05; ***P* < .01; ****P* < .001.

primary hepatocytes inhibited PAOA-induced lipid accumulation and reduced TG concentration (Figure 4*C*–*I*). A qRT-PCR analysis revealed that *OTUD5* knockdown in primary hepatocytes contributed to PAOA-induced hepatocyte lipid accumulation and inflammation. *OTUD5* overexpression in primary hepatocytes inhibited PAOA-induced hepatocyte lipid accumulation and inflammation (Figure 5*A*–*D*).

Conditional Knockout of OTUD5 in Hepatocytes Exacerbates MASH in HFHC-fed Mice

To confirm the involvement of hepatocyte OTUD5 in MASLD pathogenesis in vivo, conditional knockout of OTUD5 in hepatocytes (*Otud5*-HKO; Figure 6*A*) was generated. Western blotting confirmed that the protein expression level of OTUD5 was barely affected in other tissues (brain, lung, and colon). OTUD5 protein expression in the liver was conditionally deleted in hepatocytes but was still present in the non-parenchymal cells of *Otud5*-HKO mice (Figure 6*B* and *C*). First, primary hepatocytes were isolated from *Otud5*-HKO mice and *Otud5*-Flox mice. Isolated primary hepatocytes were stimulated with BSA/PAOA. Consistently, as indicated by Nile Red staining, no visible difference in hepatocyte lipid accumulation was observed after *OTUD5* knockout under BSA-treated conditions. Nevertheless, PAOA-induced hepatocyte lipid accumulation

in primary hepatocytes isolated from *Otud5*-HKO mice was significantly aggravated compared with that in primary hepatocytes isolated from *Otud5*-Flox mice (Figure 6*D* and *E*).

Otud5-HKO mice and *Otud5*-Flox mice were maintained for 16 weeks with NC or HFHC diet. *Otud5*-HKO mice that were fed NC diet displayed no visible differences in liver

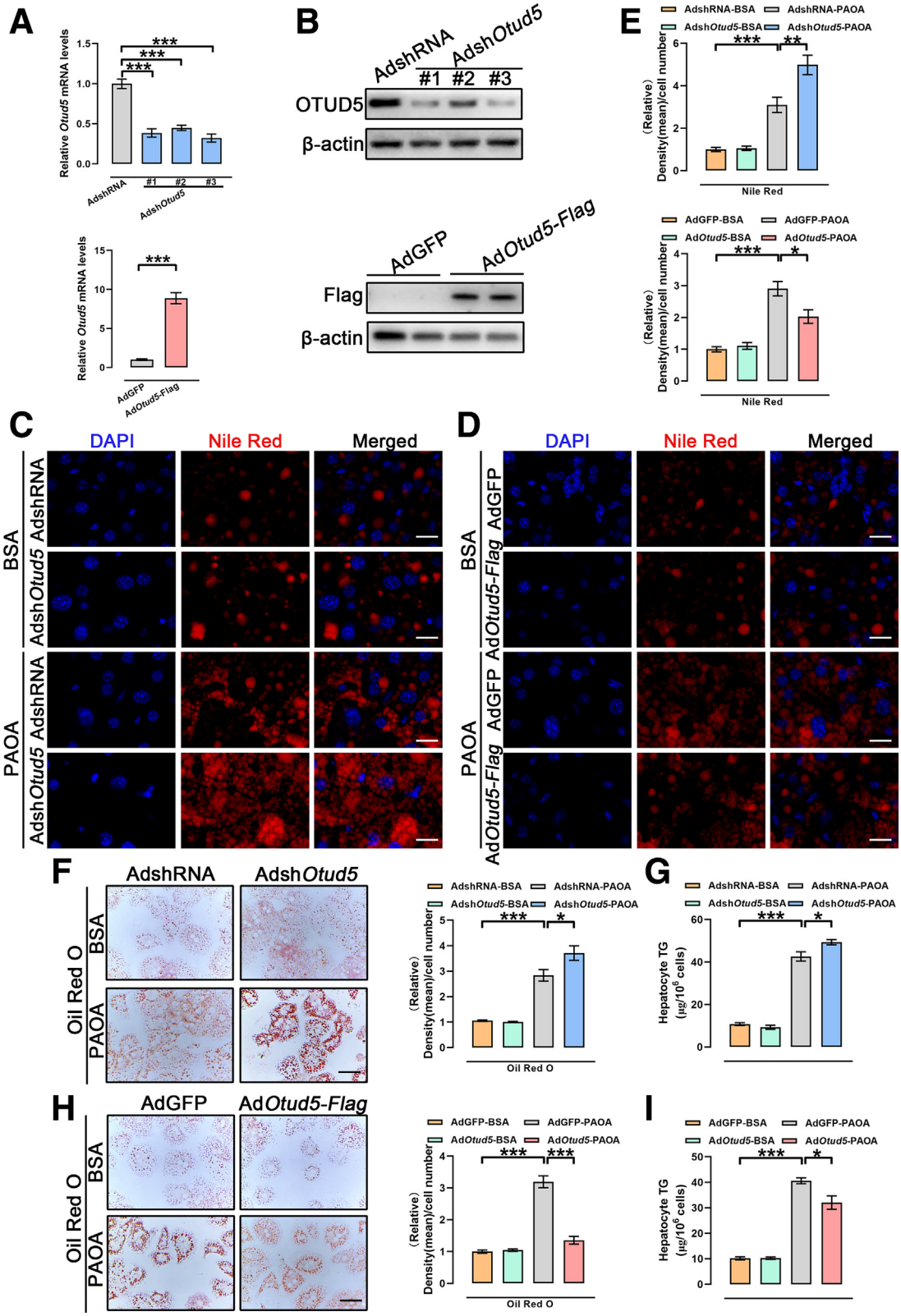

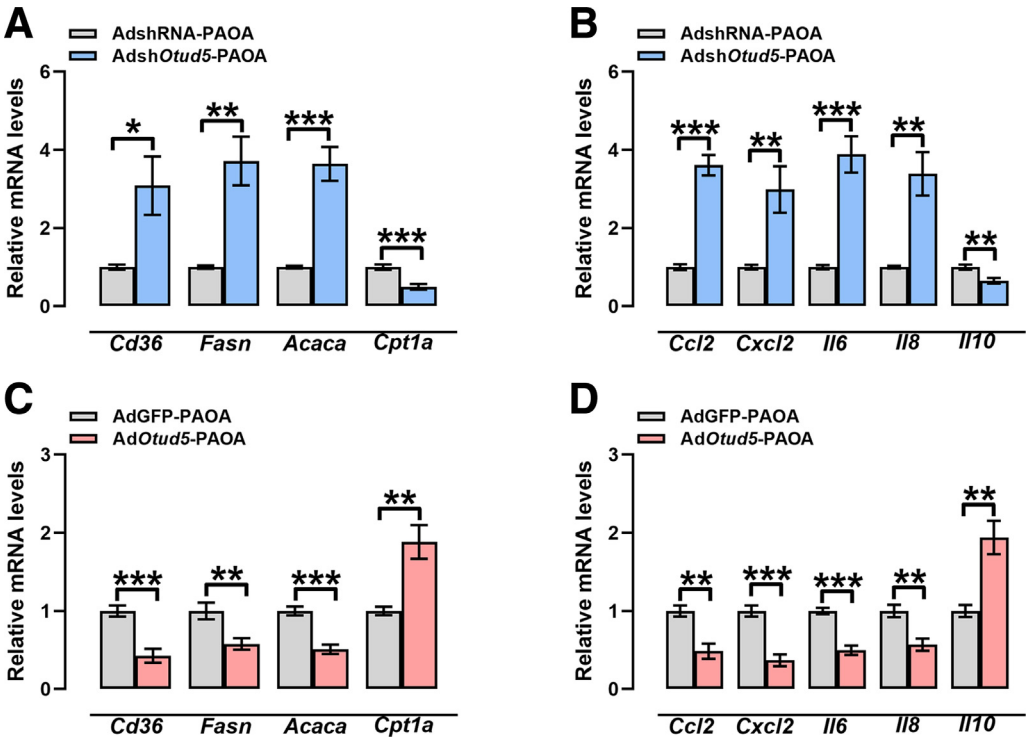

Figure 5. OTUD5 inhibits lipid accumulation and inflammation in hepatocytes. (*A* and *B*) Relative mRNA expression levels of genes with respect to fatty acid metabolism (*A*) and inflammatory cytokines and chemokines (*B*) in primary hepatocytes infected with Adsh*Otud5* or its control vector under PAOA stimulation. (*C* and *D*) Relative mRNA expression levels of genes with respect to fatty acid metabolism (*C*) and inflammatory cytokines and chemokines (*D*) in primary hepatocytes transfected with Ad*Otud5*-Flag or its control vector under PAOA stimulation. For all panels, data are presented as mean ± standard error of the mean. *P* values were calculated by two-tailed unpaired Student *t* test. **P* < .05; ***P* < .01; ****P* < .001.

weight, body weight, live/body weight ratios, insulin resistance, and hepatic steatosis compared with *Otud5*-Flox mice (Figure 7*A*–*F*). However, after 16 weeks of HFHC feeding, *Otud5*-HKO mice showed increased liver weight and liver/body weight ratios compared with *Otud5*-Flox mice (Figure 7*A* and *C*). However, *Otud5*-HKO mice displayed comparable body weights with *Otud5*-Flox mice after HFHC feeding (Figure 7*B*). Higher insulin levels and fasting blood glucose were observed in *Otud5*-HKO mice than in *Otud5*-Flox mice after HFHC feeding (Figure 7*D*). Impaired glucose tolerance in *Otud5*-HKO mice was also detected, as observed in the glucose tolerance test assays after HFHC feeding (Figure 7*E*). Furthermore, *Otud5*-HKO mice that were fed HFHC exhibited more severe hepatic steatosis than *Otud5*-Flox mice, as indicated by the hepatic TG and total cholesterol (TC) contents (Figure 7*F*), H&E staining (Figure 7*G* and *H*), and Oil Red O staining (Figure 7*I*). Consistently, *Otud5*-HKO mice up-regulated the expression of genes responsible for fatty acid intake (*Cd36*) and synthesis (*Fasn* and *Acaca*) but down-regulated the expression of genes involved in fatty acid β-oxidation (*Cpt1a*) compared with *Otud5*-Flox mice (Figure 7*J*). *Otud5*-HKO mice showed increased infiltration of $CD11b^+$ and $F4/80^+$ inflammatory cells in the liver compared with *Otud5*-Flox mice after HFHC consumption (Figure 7*K*). *Otud5*-HKO mice also showed a more severe inflammatory response than did *Otud5*-Flox mice after HFHC consumption, as indicated by hepatic mRNA expression levels of cytokines (*Ccl2*, *Cxcl2*, *Il6*, *Il8*, and *Il10*; Figure 7*L*). In addition, HFHC-fed *Otud5*-HKO mice showed more severe fibrosis, as observed by Picrosirius red and Masson staining, and increased mRNA expression levels of genes related to fibrosis (*Col1a1*, *Col3a1*, *Ctgf*, *Tgfb1*, and *α-Sma*) in the liver compared with those in

Figure 4. (***See previous page***). **OTUD5 inhibits lipid accumulation in hepatocytes.** (*A*) Expression levels of *Otud5* mRNA in primary hepatocytes infected with 3 different Adsh*Otud5* constructs or Ad*Otud5*-Flag and their control vectors. (*B*) Expression levels of OTUD5 protein in primary hepatocytes infected with 3 different Adsh*Otud5* constructs or Ad*Otud5*-Flag and their control vectors. (*C* and *D*) Representative images of Nile Red staining in isolated primary hepatocytes infected with Adsh*Otud5* or Ad*Otud5*-Flag under BSA/PAOA treatment. Scale bar: 25 μm. (*E*) Quantification of Nile Red staining density. (*F*) Left: Oil Red O staining in isolated primary hepatocytes infected with Adsh*Otud5* or its control vector under BSA/PAOA treatment. Right: quantification of Oil Red O staining density. Scale bar: 25 μm. (*G*) TG was detected in isolated primary hepatocytes infected with Adsh*Otud5* or its control vector under BSA/PAOA treatment. (*H*) Left: Oil Red O staining in isolated primary hepatocytes infected with Ad*Otud5*-Flag or its control vector under BSA/PAOA treatment. Right: quantification of Oil Red O staining density. Scale bar: 25 μm. (*I*) TG was detected in isolated primary hepatocytes infected with Ad*Otud5*-Flag or its control vector under BSA/PAOA treatment. For all panels, data are presented as mean ± standard error of the mean. *P* values were calculated by two-tailed unpaired Student *t* test. **P* < .05; ***P* < .01; ****P* < .001.

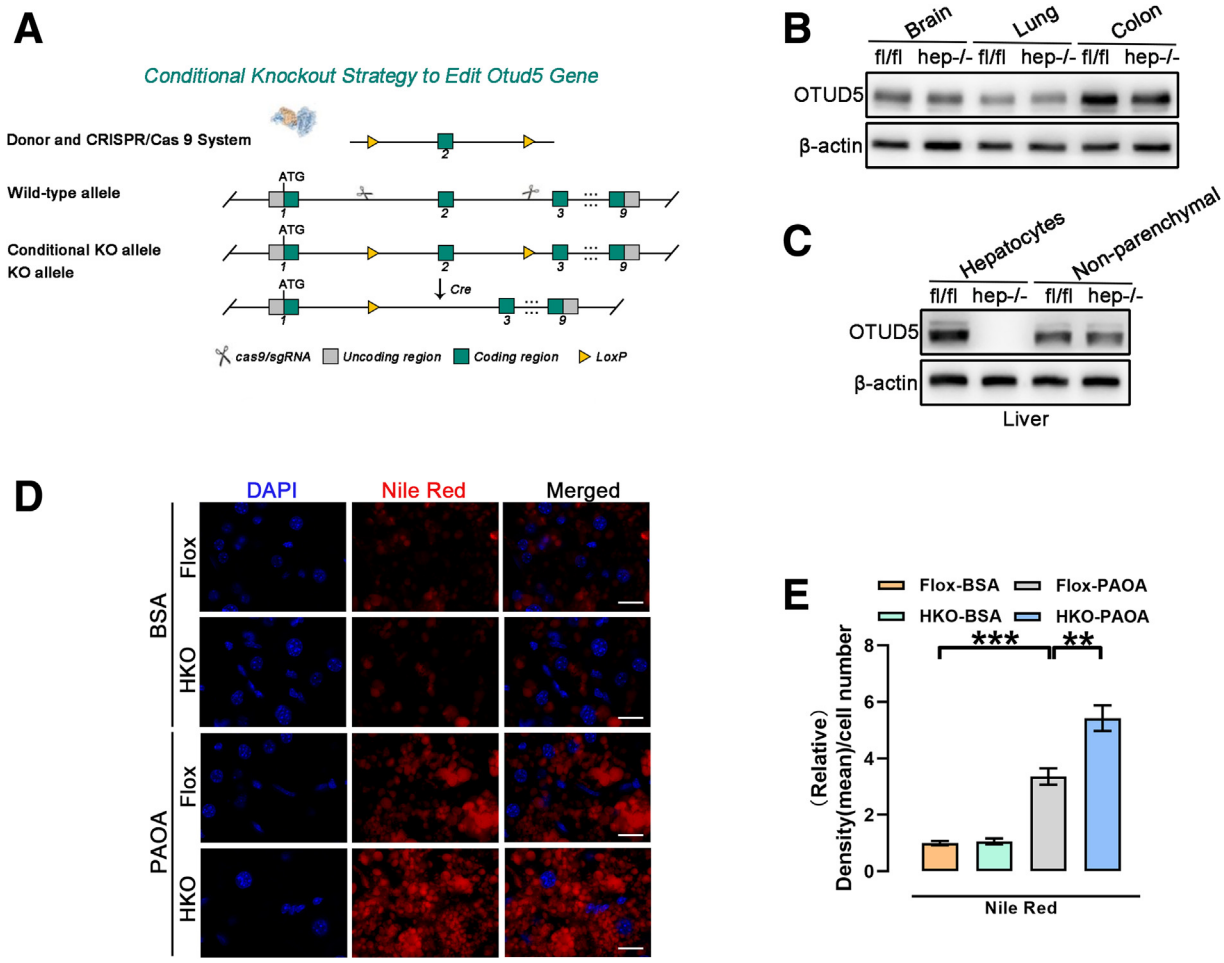

Figure 6. OTUD5 knockout aggravated hepatocyte lipid accumulation. (*A*) Knockout strategy to edit the *OTUD5* gene. (*B*) OTUD5 protein expression in brain, lung, and colon of *Otud5*-HKO and *Otud5*-Flox mice using Western blot. (*C*) OTUD5 protein expression in primary hepatocytes and nonparenchymal cells of *Otud5*-HKO and *Otud5*-Flox mice using Western blot. (*D*) Representative images of Nile Red staining in isolated primary hepatocytes from *Otud5*-HKO mice and *Otud5*-Flox mice under BSA/PAOA treatment. Scale bar: 25 μm. (*E*) Quantification of Nile Red staining density. For all panels, data are presented as mean ± standard error of the mean (n = 6 independent experiments). *P* values were calculated by two-tailed unpaired Student *t* test. $^{**}P < .01$; $^{***}P < .001$.

Otud5-Flox mice (Figure 7*M* and *N*). Furthermore, compared with those in *Otud5*-Flox mice, the concentrations of serum ALT and AST were markedly elevated in HFHC-fed *Otud5*-HKO mice (Figure 7*O*).

Conditional Knockout of OTUD5 in Hepatocytes Exacerbated HFF-induced MASH

Considering the heterogeneity of MASH, we further examined OTUD5 function on a HFF diet-induced MASH model that renders relatively more severe fibrosis than does the HFHC model.[40] *Otud5*-HKO mice fed NC diet displayed no visible difference in liver weight, body weight, liver/body weight ratios, insulin resistance, or hepatic steatosis compared with *Otud5*-Flox mice (Figure 8*A*–*F*). However, consistent with the findings observed in the HFHC model, *Otud5*-HKO mice showed higher liver weight and liver/body weight ratios without any significant effects on body weight (Figure 8*A* and *C*) after HFF consumption compared with *Otud5*-Flox mice. HFF-fed *Otud5*-HKO mice showed higher insulin levels and fasting blood glucose levels than *Otud5*-Flox mice (Figure 8*D*). Impaired glucose tolerance in HFF-fed *Otud5*-HKO mice was confirmed using glucose tolerance test (Figure 8*E*). Increased TG and TC contents (Figure 8*F*), accompanied by the NAS scores (Figure 8*G* and *H*), steatosis (Figure 8*I* and *J*), inflammation (Figure 8*K* and *L*), and fibrosis (Figure 8*M* and *N*), were also observed in the livers of *Otud5*-HKO mice compared with *Otud5*-Flox mice after 16 weeks of HFF feeding. Finally, the HFF diet induced more severe liver injury in HFF-fed *Otud5*-HKO mice, as indicated by the increased serum ALT and AST levels compared with *Otud5*-Flox mice (Figure 8*O*).

OTUD5 Interacts With VDAC2 and Cleaves the K48-linked Polyubiquitin Chains From VDAC2

To identify the specific target of OTUD5 in suppressing hepatocyte lipid accumulation and inflammation, we

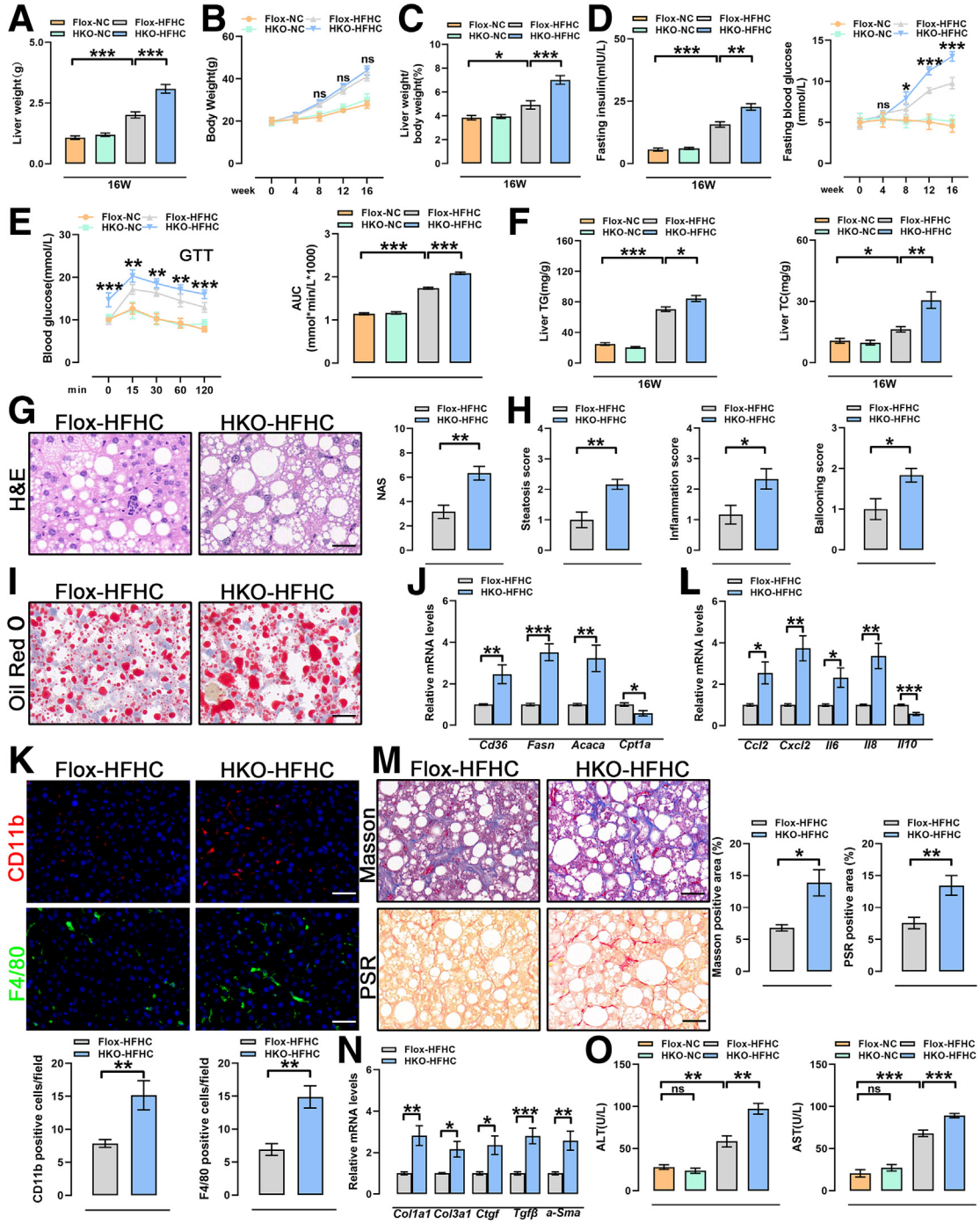

Figure 7. Conditional knockout of OTUD5 in hepatocytes contributes to HFHC-induced MASH. (*A*) Liver weights of NC or HFHC-fed *Otud5*-HKO and *Otud5*-Flox mice. (*B*) Body weights of NC or HFHC-fed *Otud5*-HKO and *Otud5*-Flox mice. (*C*) Liver/body weight ratios of NC or HFHC-fed *Otud5*-HKO and *Otud5*-Flox mice. (*D*) Fasting serum insulin (left) and blood glucose (right) levels in NC or HFHC-fed *Otud5*-HKO and *Otud5*-Flox mice. (*E*) Left: glucose tolerance test (GTT) assay was used in NC or HFHC-fed *Otud5*-HKO and *Otud5*-Flox mice. Right: the area under the curve (AUC) was calculated. (*F*) Hepatic TG and TC concentrations in NC or HFHC-fed *Otud5*-HKO and *Otud5*-Flox mice. (*G*) H&E-stained liver sections of HFHC-fed *Otud5*-HKO and *Otud5*-Flox mice. NAS score was calculated. Scale bar: 50 μm. (*H*) Scores of hepatic steatosis, inflammation, and ballooning were quantified respectively. (*I*) Oil Red O–stained liver sections of HFHC-fed *Otud5*-HKO and *Otud5*-Flox mice. (*J*) Relative mRNA expression levels of genes with respect to fatty acid metabolism in livers of HFHC-fed *Otud5*-HKO and *Otud5*-Flox mice. (*K*) Upper: immunofluorescence images of CD11b (*red*) and F4/80 (*green*) in livers of HFHC-fed *Otud5*-HKO and *Otud5*-Flox mice. Lower: percentages of $CD11b^+$ cells and $F4/80^+$ cells were quantified. Scale bar: 50 μm. (*L*) Relative mRNA expression levels of inflammatory genes in livers of HFHC-fed *Otud5*-HKO and *Otud5*-Flox mice. (*M*) Left: Masson (upper) and Picrosirius red (PSR; lower)-stained livers of HFHC-fed *Otud5*-HKO and *Otud5*-Flox mice. Scale bar: 50 μm. Right: quantification of Masson and PSR positive cells. (*N*) Relative mRNA expression levels of genes related to fibrosis in livers of HFHC-fed *Otud5*-HKO and *Otud5*-Flox mice. (*O*) Serum ALT and AST concentrations of HFHC-fed *Otud5*-HKO and *Otud5*-Flox mice. For all panels, data are presented as mean ± standard error of the mean (n = 6 mice/group). *P* values were calculated by two-tailed unpaired Student *t* test. **P* < .05; ***P* < .01; ****P* < .001; ns, not significant.

performed immunoprecipitation (IP) mass spectrometry analysis using OTUD5-overexpressing HepG2 cells. Quantitative proteomics was also performed to screen for dysregulated proteins upon OTUD5 overexpression (Figure 9*A*). Afterwards, we integrated the results of IP mass spectrometry and quantitative proteomics. Three candidates

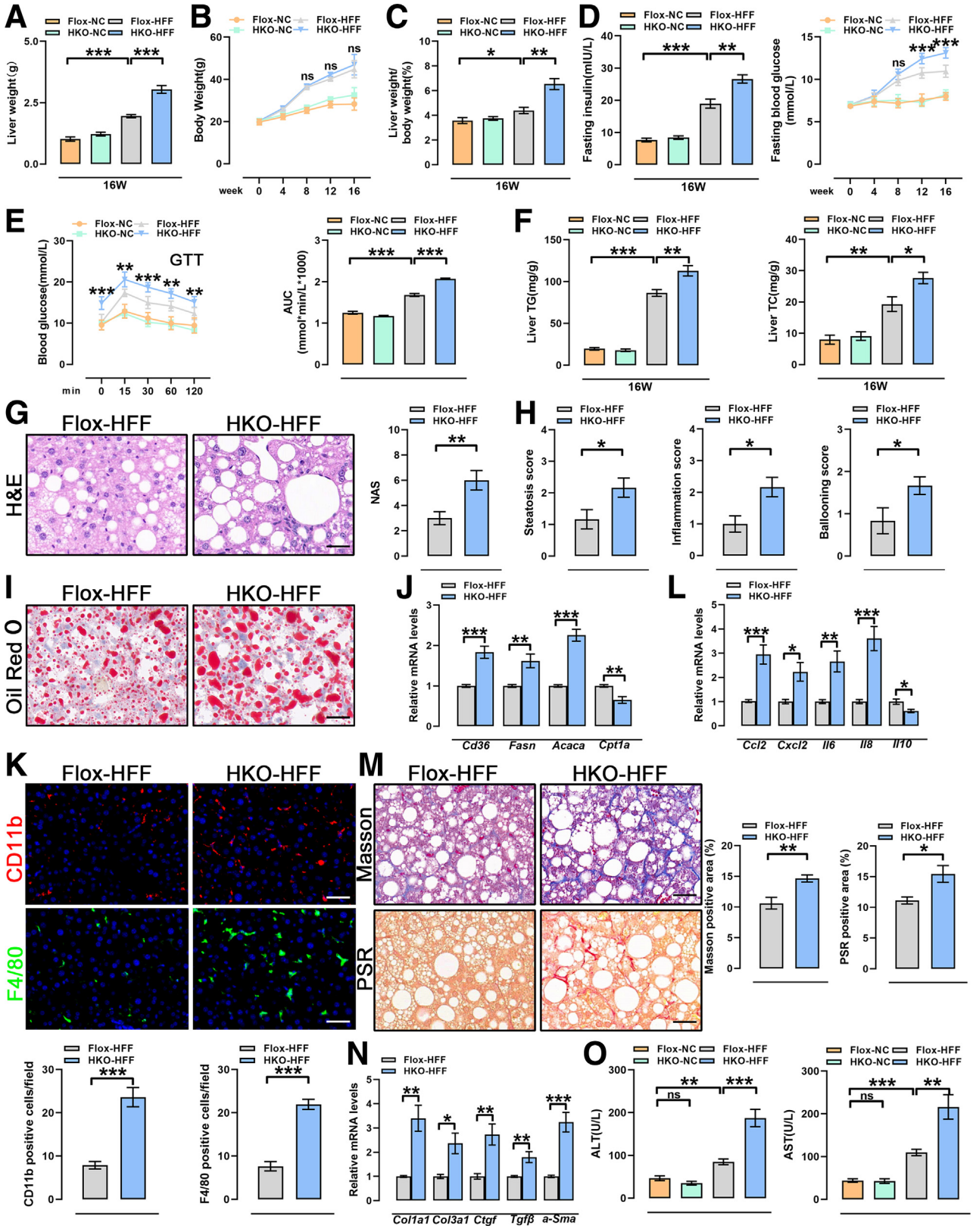

were identified with VDAC2 showing obvious up-regulation (Figure 9*B*). Thus, we hypothesized that VDAC2 may serve as an interacting protein with OTUD5. We determined the expression of VDAC2 in normal human livers without steatosis and in those with simple steatosis or MASH. Hepatic VDAC2 protein levels were significantly lower in livers with simple steatosis or MASH than in normal human livers. Moreover, human livers with MASH had lower VDAC2 protein levels than those with simple steatosis (Figure 9*C*). Pearson correlation analysis also revealed that OTUD5 protein levels were positively correlated with VDAC2 protein levels (Figure 9*D*). Consistent with our findings in human individuals, VDAC2 protein levels were evidently decreased in mouse livers with HFHC or HFF diets compared with the levels in their littermates that were fed NC diet (Figure 9*E* and *F*). Similarly, VDAC2 protein levels decreased in isolated primary mouse hepatocytes and HepG2 cells in the presence of PAOA compared with BSA-treated control cells (Figure 9*G* and *H*).

Immunofluorescence staining assays using confocal microscopy were then performed in HEK-293T cells, and a distinct interaction between OTUD5 and VDAC2 was detected (Figure 10*A*). This interaction was validated by reciprocal coimmunoprecipitation assays (Figure 10*B*). Moreover, the direct interaction between OTUD5 and VDAC2 was confirmed using glutathione S-transferase precipitation assays (Figure 10*C*). Molecular mapping assays indicated that the OTU domain of OTUD5 (213-341aa) was involved in its direct interaction with the N-terminal domain of VDAC2 (1-36aa) (Figure 10*D*–*F*). In addition, HA-tagged OTUD5 D2 (OTU domain) and His-tagged VDAC2 D1 (N-terminal domain) were immunoprecipitated (Figure 10*G*). OTU domain-deleted OTUD5 was also constructed and used to infect primary mouse hepatocytes. However, its overexpression failed to mitigate lipid accumulation (Figure 11*A*–*F*). Collectively, these data indicate that OTUD5 directly interacts with VDAC2 in an OTU domain-dependent manner.

OTUD5 is known to regulate the deubiquitination and stability of interacting proteins; hence, we tested whether OTUD5 mediated the stabilization of VDAC2. Western blotting analysis revealed that OTUD5 extended the half-life of endogenous VDAC2 (Figure 12*A*). VDAC2 can be modified and degraded by ubiquitination.[41] We found that the *OTUD5* knockdown-mediated decrease in VDAC2 expression level was abolished by MG132, supporting that OTUD5 restrained the proteasomal degradation of VDAC2 (Figure 12*B*). Consistently, we found that OTUD5 suppressed ubiquitination of both endogenous and exogenous VDAC2 in PAOA-treated HepG2 cells (Figure 12*C* and *D*). Conversely, isolated primary hepatocytes from *Otud5*-HKO mice that lacked OTUD5 expression displayed increased ubiquitination of VDAC2 (Figure 12*E*). Thus, we hypothesized that the effects of OTUD5 on VDAC2 ubiquitination rely on its enzymatic activity. We constructed a catalytically inactive OTUD5 mutant (C224S), whose cysteine at position 224 was mutated to serine and was deficient in deubiquitination activity. Flag-VDAC2 and HA-OTUD5 or its catalytically inactive mutant C224S were cotransfected into HepG2 cells; we found that WT OTUD5 rather than mutant C224S resulted in a marked decrease in VDAC2 ubiquitination, demonstrating that the enzymatic activity of OTUD5 was essential for the deubiquitination of VDAC2 (Figure 12*F*). Because diverse types of ubiquitin chains play different roles in modulating protein function, we explored the form of VDAC2 ubiquitination that is regulated by OTUD5. Flag-VDAC2, HA-Ub, or its site mutants, with or without HA-OTUD5, were co-transfected into HepG2 cells. The data revealed that OTUD5 decreased the ubiquitination level of VDAC2 in cells transfected with K48O (Ub with the intact Lys48 residue alone), rather than K6O, K11O, K27O, K29O, K33O, or K63O (Figure 12*G*). More importantly, OTUD5 exhibited a negligible effect on the ubiquitination level of VDAC2 in cells transfected with the ubiquitin mutant K48R, but the levels were down-regulated in cells transfected with WT ubiquitin and K48O ubiquitin, demonstrating that OTUD5 separates the K48-linked ubiquitination from VDAC2 but not other forms of polyubiquitin chains (Figure 12*H*). Because VDAC2 mainly interacts with OTUD5 via the N-terminal stretch, we hypothesized that OTUD5 likely modulates the ubiquitination of lysine residues (s) in the N-terminal stretch of VDAC2. Deubiquitination assays were

Figure 8. (***See previous page***). **Conditional knockout of OTUD5 in hepatocytes aggravates HFF-induced MASH.** (*A*) Liver weights of NC or HFF-fed *Otud5*-HKO and *Otud5*-Flox mice. (*B*) Body weights of NC or HFF-fed *Otud5*-HKO and *Otud5*-Flox mice. (*C*) Liver/body weight ratios of NC or HFF-fed *Otud5*-HKO and *Otud5*-Flox mice. (*D*) Fasting serum insulin (left) and blood glucose (right) levels in NC or HFF-fed *Otud5*-HKO and *Otud5*-Flox mice. (*E*) Left: glucose tolerance test (GTT) assay was used in NC or HFF-fed *Otud5*-HKO and *Otud5*-Flox mice. Right: the area under the curve (AUC) was calculated. (*F*) Hepatic TG and TC concentrations in NC or HFF-fed *Otud5*-HKO and *Otud5*-Flox mice. (*G*) H&E-stained liver sections of HFF-fed *Otud5*-HKO and *Otud5*-Flox mice. NAS score was calculated. Scale bar: 50 μm. (*H*) Scores of hepatic steatosis, inflammation, and ballooning were quantified respectively. (*I*) Oil Red O–stained liver sections of HFF-fed *Otud5*-HKO and *Otud5*-Flox mice. (*J*) Relative mRNA expression levels of genes with respect to fatty acid metabolism in livers of HFF-fed *Otud5*-HKO and *Otud5*-Flox mice. (*K*) Upper: immunofluorescence images of CD11b (*red*) and F4/80 (*green*) in livers of HFF-fed *Otud5*-HKO and *Otud5*-Flox mice. Lower: percentages of $CD11b^+$ and $F4/80^+$ cells were quantified. Scale bar: 50 μm. (*L*) Relative mRNA expression levels of inflammatory genes in livers of HFF-fed *Otud5*-HKO and *Otud5*-Flox mice. (*M*) Left: Masson (upper) and Picrosirius red (PSR) (lower) staining in livers of HFF-fed *Otud5*-HKO and *Otud5*-Flox mice. Scale bar: 50 μm. Right: quantification of Masson and PSR positive cells. (*N*) Relative mRNA expression levels of genes related to fibrosis in livers of HFF-fed *Otud5*-HKO and *Otud5*-Flox mice. (*O*) Serum ALT and AST concentrations of HFF-fed *Otud5*-HKO and *Otud5*-Flox mice. For all panels, data are presented as mean ± standard error of the mean (n = 6 mice/group). *P* values were calculated by two-tailed unpaired Student *t* test. $^*P < .05$; $^{**}P < .01$; $^{***}P < .001$; ns, not significant.

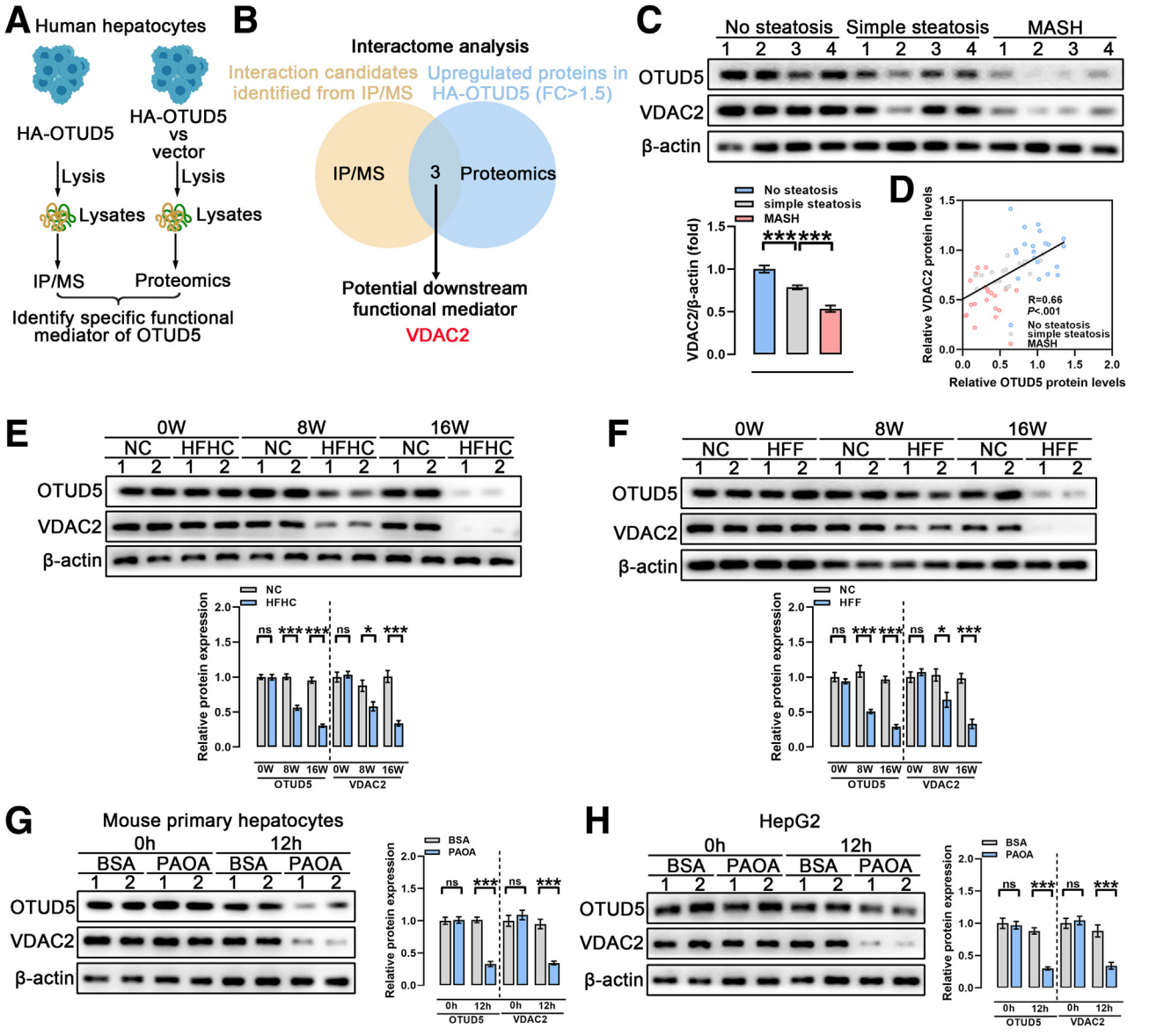

Figure 9. VDAC2 expression is decreased in fatty liver. (*A*) Schema displaying the procedure of investigating downstream targets of OTUD5 by intersection analysis of IP-MS and quantitative proteomics. (*B*) Interactome analysis of IP/mass spectrometry and quantitative proteomics. (*C*) Representative Western blot analysis and quantification of VDAC2 expression in normal human livers (n = 20) and those with simple steatosis (n = 20) or MASH (n = 20). (*D*) Pearson analysis of correlation between OTUD5 protein levels and VDAC2 protein levels. (*E*) Upper: representative Western blots analysis of VDAC2 protein levels in livers of C57BL/6J mice with NC diet or HFHC diet for indicated weeks. n = 6 mice/group. Lower: quantification of Western blot analysis of VDAC2 protein levels in livers of C57BL/6J mice with NC diet or HFHC diet for indicated weeks. n = 6 mice/group. (*F*) Upper: representative Western blots analysis of VDAC2 protein levels in livers of C57BL/6J mice with NC diet or HFF diet for indicated weeks. n = 6 mice/group. Lower: quantification of Western blot analysis of VDAC2 protein levels in livers of C57BL/6J mice with NC diet or HFF diet for indicated weeks. n = 6 mice/group. (*G*) Left: VDAC2 protein levels in primary hepatocytes stimulated with BSA or PAOA. Right: quantification of Western blot analysis of VDAC2 protein levels in primary hepatocytes stimulated with BSA or PAOA. (*H*) Left: VDAC2 protein levels in HepG2 cells stimulated with BSA or PAOA. Right: quantification of Western blot analysis of VDAC2 protein levels in HepG2 cells stimulated with BSA or PAOA. For all panels, n represents biologically independent repeats. *P* values were calculated by two-tailed unpaired Student *t* test. **P* < .05; ****P* < .001; ns, not significant.

performed with WT VDAC2 and its different KR mutants, in which the lysine residues in the N-terminal stretch (K23 and K31) were mutated to arginine, individually and in combination. The results showed that both individual and combination mutants of VDAC2 resisted OTUD5-mediated deubiquitination (Figure 12*I*). Consistently, OTUD5 overexpression did not affect the half-life of VDAC2-2KR, suggesting that OTUD5 mainly deubiquitinated VDAC2 at K23 and K31 (Figure 12*J*). Collectively, these data validated that OTUD5 sustains the stability of

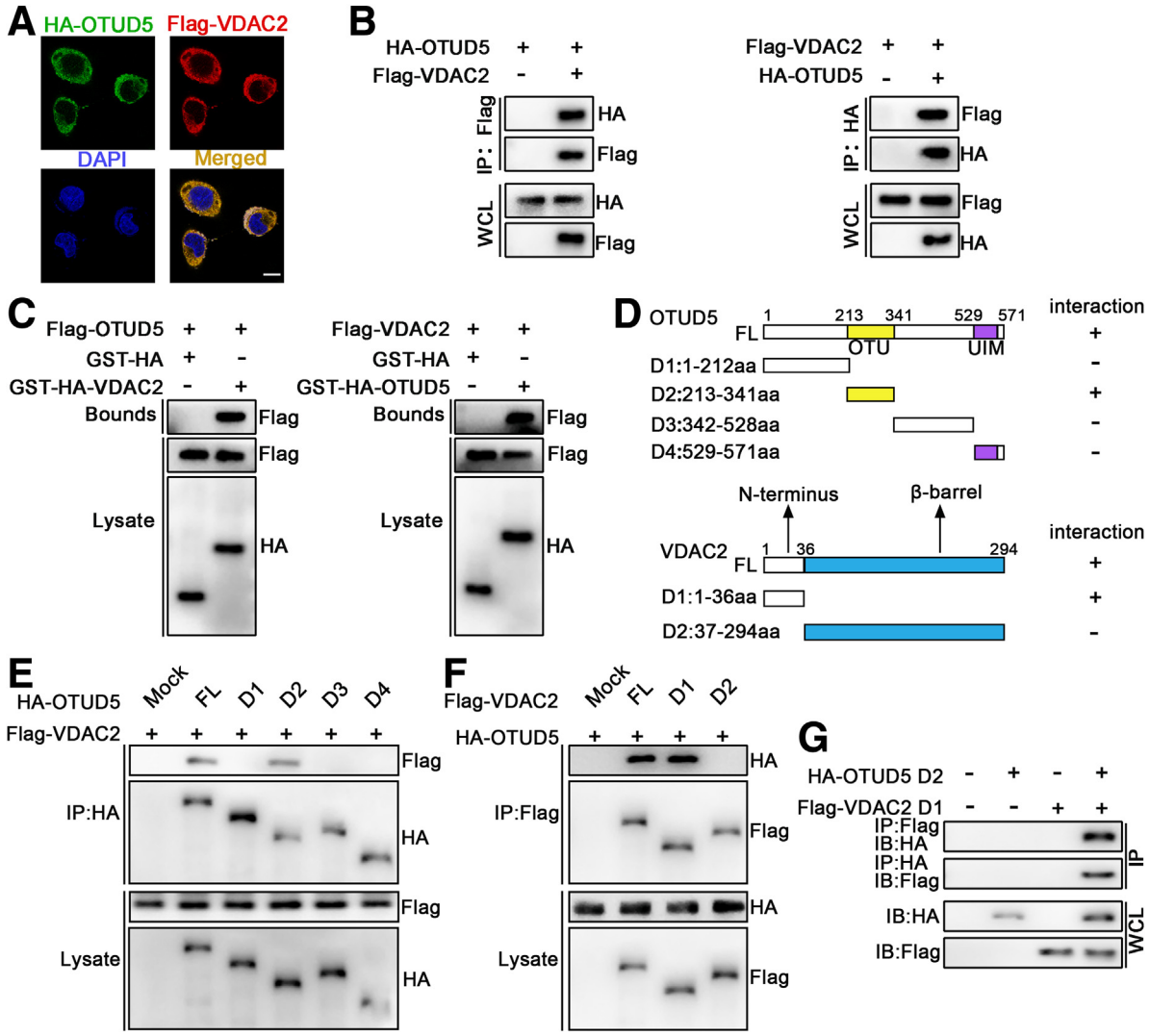

Figure 10. OTUD5 directly interacts with VDAC2. (*A*) Confocal microscopy images displaying co-localization of HA-OTUD5 (*green*) and Flag-VDAC2 (*red*) in HEK-293T cells. Scale bar, 10 μm. (*B*) Co-IP assays showing interaction of HA-OTUD5 and Flag-VDAC2 in HEK-293T cells. (*C*) Glutathione S-transferase (GST) precipitation assays indicating direct binding of OTUD5 and VDAC2. (*D*) Interaction domains of OTUD5 and VDAC2 were designed using full-length and truncated OTUD5 (upper) and VDAC2 (bottom) expression constructs. FL, full-length. (*E* and *F*) Molecular mapping assays detecting interaction domains of OTUD5 and VDAC2 in HEK-293T cells transfected with the plasmids expressing full-length and truncations of OTUD5 and VDAC2. (*G*) Co-IP experiments revealed interaction of HA-OTUD5 D2 and Flag-VDAC2 D1. n = 3 independent experiments.

VDAC2 by separating the K48-linked polyubiquitin chains from VDAC2 K23 and K31.

VDAC2 Mediates the Effect of OTUD5 on Lipid Accumulation and Mitochondrial Homeostasis in Hepatocytes

Because VDAC2 has been identified as the binding partner of OTUD5, we wondered whether the OTUD5-mediated protective effect on lipid accumulation is mediated by VDAC2. Primary hepatocytes were infected with an adenovirus-mediated *VDAC2* overexpression vector (Ad*Vdac2*-Flag; Figure 13*A* and *B*). Notably, *VDAC2* overexpression impaired the PAOA-induced lipid accumulation and inflammatory response in hepatocytes. Meanwhile, the anabolic effects of *OTUD5* knockdown on PAOA-induced hepatocyte lipid accumulation were effectively reversed by *VDAC2* overexpression (Figure 13*C*–*E*). Moreover, the dysregulated lipogenic and inflammatory genes induced by *OTUD5* knockdown were reversed when *VDAC2* was overexpressed (Figure 13*F* and *G*).

Considering the vital function of VDAC2 in mitochondrial functions and the pivotal role of mitochondria in MASLD pathogenesis,[42] we wondered whether OTUD5-induced mitigation of hepatic steatosis is dependent on its regulation of mitochondrial functions. Therefore, we performed a metabolic flux analysis in primary hepatocytes using [^{13}C] glucose as the substrate (Figure 14*A* and *B*). Metabolic tracking revealed that *OTUD5* knockdown induced a significantly decreased abundance of tricarboxylic acid (TCA) cycle metabolites (such as M2 citrate, M2 ketoglutarate, M2 succinate, and M2 fumarate), with

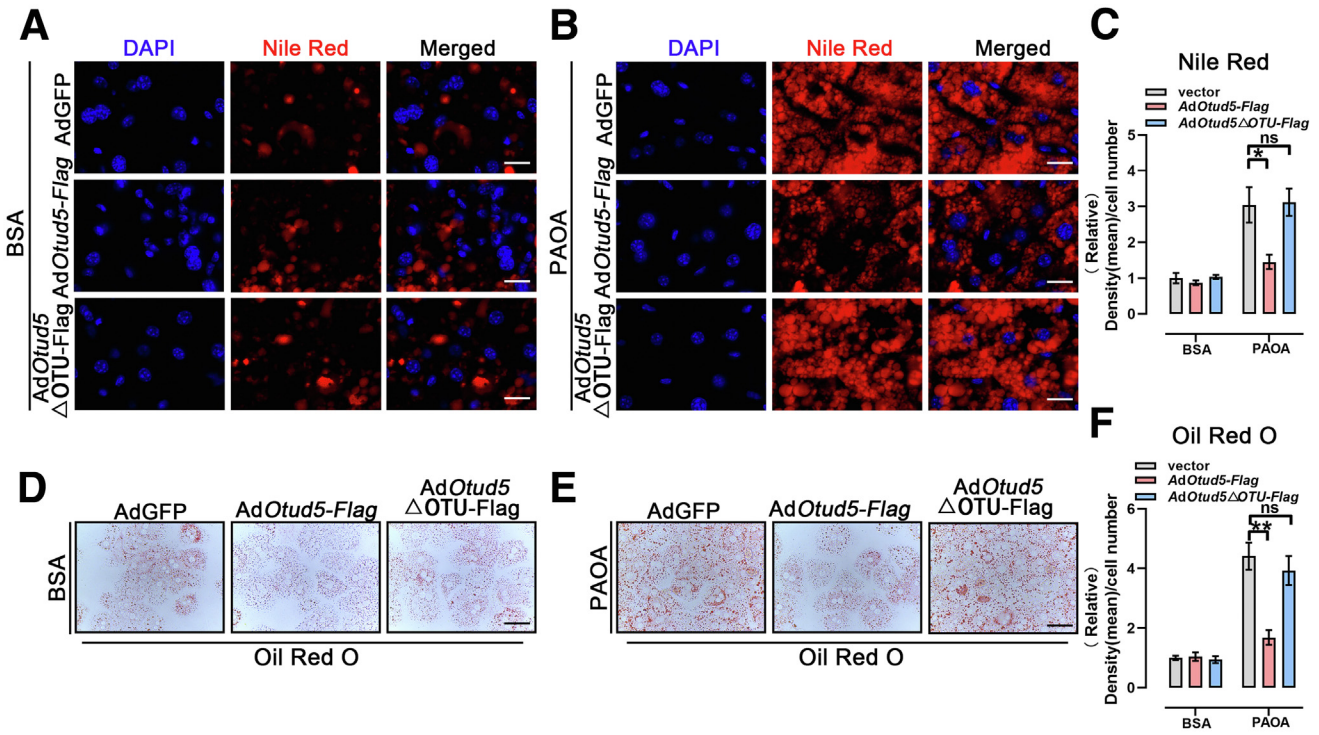

Figure 11. OTUD5 alleviates MASH in an OTU domain-dependent manner. (*A* and *B*) Nile Red staining in isolated primary hepatocytes infected with AdGFP, Ad*Otud5*-Flag, or Ad*Otud5*ΔOTU-Flag under BSA/PAOA treatment. Scale bar: 25 μm. (*C*) Quantification of Nile Red staining density. (*D* and *E*) Oil Red O staining in isolated primary hepatocytes infected with AdGFP, Ad*Otud5*-Flag, or Ad*Otud5*ΔOTU-Flag under BSA/PAOA treatment. Scale bar: 25 μm. (*F*) Quantification of Oil Red O staining density. For all panels, data are presented as mean ± standard error of the mean (n = 3 independent experiments). *P* values were calculated by two-tailed unpaired Student *t* test. $^{*}P < .05$; $^{**}P < .01$; ns, not significant.

a compensatory increase in the abundance of glycolytic metabolites (such as M6 G-6-P, M6 F-6-P, M6 F-1, 6-P, M3 pyruvate, and M3 lactate). In contrast, *VDAC2* overexpression induced a significant increase in the abundance of TCA cycle metabolites and a decreased abundance of glycolytic metabolites. Importantly, mitochondrial dysfunction induced by *OTUD5* knockdown was abolished by *VDAC2* overexpression in PAOA-stimulated primary hepatocytes (Figure 14*C* and *D*). Oxygen consumption rates were also measured, and the results revealed that *OTUD5* knockdown-induced impaired mitochondrial respiratory capacity was reversed by *VDAC2* overexpression (Figure 14*E*). Transmission electron microscopy indicated that *OTUD5* knockdown altered the mitochondrial morphology in PAOA-stimulated primary hepatocytes. *OTUD5* knockdown resulted in the transformation of the apoptotic mitochondrial phenotype: swelling, rounding, and increased fission. Nevertheless, *VDAC2* overexpression nearly normalizes mitochondrial morphology. *VDAC2* overexpression restored *OTUD5* knockdown induced transformation of mitochondrial morphology (Figure 14*F*). JC-1 staining, which detects mitochondrial membrane potential via fluorescence, consistently demonstrated that *OTUD5* knockdown decreased mitochondrial membrane potential under PAOA treatment in primary hepatocytes. Meanwhile, the decreased mitochondrial membrane potential resulting from *OTUD5* knockdown was reversed by VDAC2 overexpression in PAOA-stimulated primary hepatocytes (Figure 14*G*). Altogether, these data validate that VDAC2 is indispensable for OTUD5 to mediate its protection against hepatic steatosis by maintaining mitochondrial function.

Adeno-associated Virus–induced Otud5 Overexpression Inhibited HFF-induced MASH

Finally, the therapeutic efficacy of *Otud5* was evaluated in the MASH model. Adeno-associated virus (AAV)8 expressing *Otud5* (AAV-*Otud5*) was injected into 8-week-old HFF-fed mice, which were then fed the HFF diet for another 8 weeks (Figure 15*A* and *B*). No significant difference in body weight was observed between the AAV-*Otud5* and AAV-GFP groups (Figure 15*C*). Nevertheless, the results revealed that AAV-*Otud5* injection decreased liver weight, liver/body weight ratios, and fasting blood glucose levels after HFF feeding for 16 weeks compared with AAV-GFP injection (Figure 15*D*–*F*). Furthermore, AAV-*Otud5* injection markedly attenuated HFF-induced hepatic lipid accumulation, inflammation, and fibrosis (Figure 15*G*–*P*). Moreover, *Otud5* re-expression also reduced serum AST and ALT levels after 16 weeks of HFF feeding compared with AAV-GFP injection (Figure 15*Q*).

Discussion

Often occurring along with metabolic and cardiovascular disorders, MASLD is the most prevalent liver disease

worldwide.[43,44] In our study, we found that OTUD5 plays a vital role in ameliorating MASLD progression. *OTUD5* knockout/knockdown markedly contributed to hepatic steatosis, inflammation, and fibrosis under metabolic stress in both in vivo and in vitro models. In contrast, *OTUD5* overexpression markedly ameliorated these hepatic

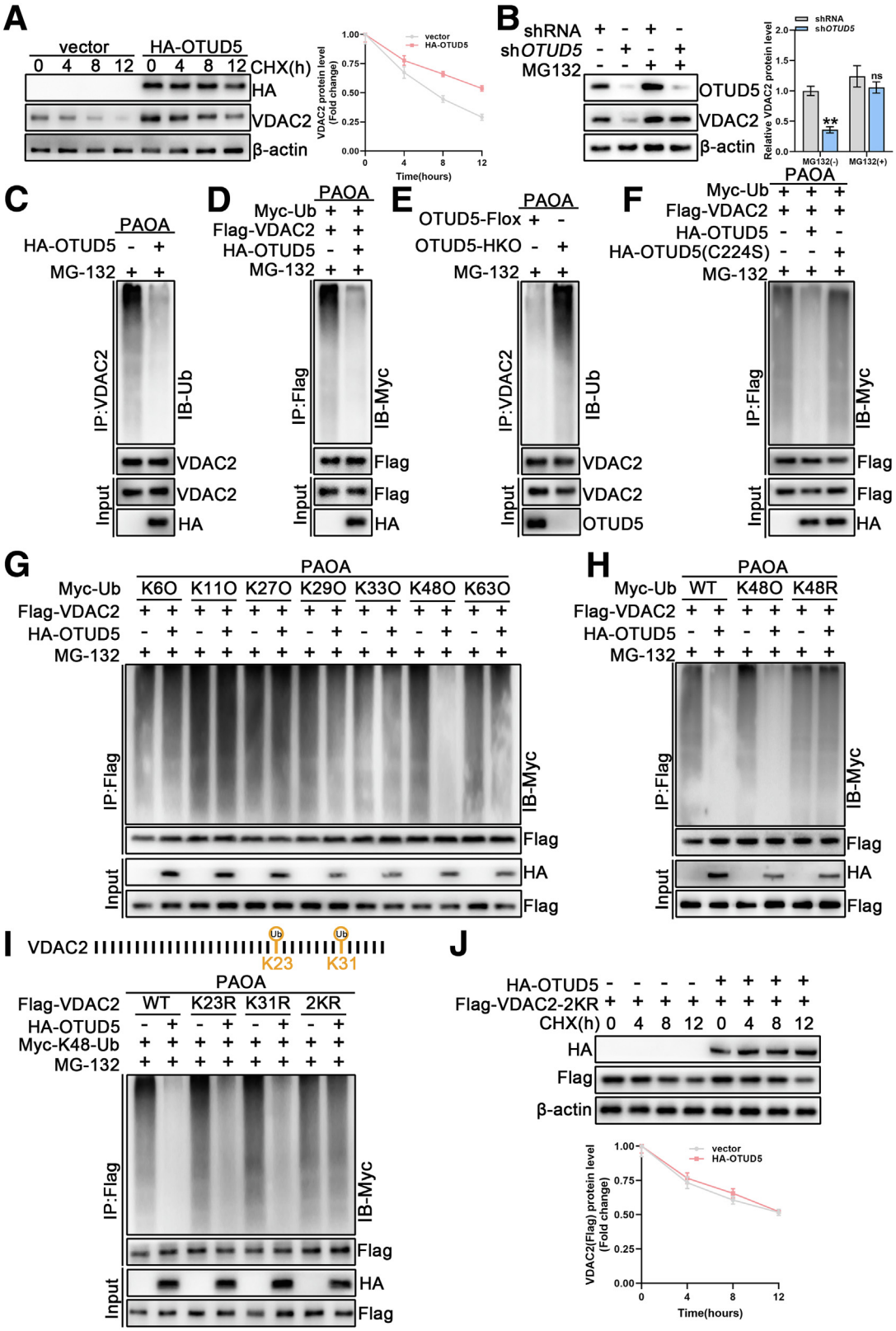

phenotypes. Mechanistically, VDAC2 mediates the inhibitory effects of OTUD5 on hepatocytes under metabolic stress. Our data also revealed that OTUD5 separated the K48-linked polyubiquitin chains from VDAC2 to maintain its stability. Importantly, the cytoprotective function of OTUD5 was confirmed using an AAV8-mediated therapeutic model. Because AAV-mediated gene replacement, editing, and silencing are becoming leading platforms in preclinical and clinical situations, AAV-mediated *OTUD5* up-regulation may be an effective strategy for mitigating the progression of MASLD.

Through the interactome, we identified VDAC2 as a binding partner of OTUD5. OTUD5 directly interacts with VDAC2 in an OTU domain-dependent manner and sustains VDAC2 stability by cleaving K48-linked polyubiquitin chains from VDAC2 K23 and K31. The VDACs family consists of 3 proteins that are localized to the mitochondrial outer membrane and participates in the transport of metabolites and ions across the mitochondrial outer membrane.[41,45] VDAC knockdowns using siRNA affects mitochondrial metabolism and results in mitochondrial dysfunction, eventually leading to apoptosis. Dysregulated VDAC expression frequently results in suppression of the substrate transport into mitochondria, reduction of the generation and release of adenosine triphosphate, induction of mitochondrial depolarization, and restraint of fatty acid oxidation.[42,46] These biological processes play vital roles in the pathogenesis of MASLD. Among the VDACs family, VDAC2 was specifically reported to be required for the effects of mitochondrial antiviral signaling protein-mediated protection against mitochondrial dysfunction and MASH.[42] Hence, it is reasonable to postulate that VDAC2 is involved in the OTUD5 effect on MASLD progression. Herein, *OTUD5* knockdown consistently and significantly decreased the levels of TCA-cycle metabolites with a compensatory increase in the levels of glycolytic metabolites. In contrast, *VDAC2* overexpression resulted in increased levels of TCA-cycle metabolites and decreased levels of glycolytic metabolites. In particular, *OTUD5* knockdown-induced mitochondrial dysfunction was abolished in the presence of *VDAC2* in PAOA-stimulated primary hepatocytes. Hence, VDAC2 is indispensable for the inhibitory effects of OTUD5 on hepatic steatosis and the maintenance of mitochondrial homeostasis.

In conclusion, we demonstrated that OTUD5 inhibited ubiquitination-mediated degradation of VDAC2 and maintained mitochondrial homeostasis, subsequently ameliorating MASLD progression. Our study identified OTUD5 as a promising therapeutic target for MASLD treatment.

Materials and Methods

Human Liver Specimens

Sixty human liver specimens were obtained from individuals who had undergone liver biopsy. Two pathologists independently evaluated the NAS in a blinded manner according to the NASH-CRN scoring system.[47] The normal samples had NAS of 0. The simple steatosis group included patients with NAS of 1–2 without ballooning or fibrosis. The MASH group included patients with NAS >4 or with NAS of 3–4 but with fibrosis. The study design was approved by the ethics committee of the First Affiliated Hospital of Nanjing Medical University. Written informed consent was obtained from all participants.

HFHC and HFF Diet-induced MASH Mice Models

Male 6- to 8-week-old C57BL/6 mice were fed HFHC diet (44% carbohydrates, 42% fat, 14% protein, and 0.2% cholesterol) for 16 weeks to establish the HFHC diet-induced MASH model. Another set of male mice were fed HFHC diet, together with 42 g/L of carbohydrate mixed in drinking water at a ratio of 55% fructose and 45% sucrose by weight for 16 weeks to establish the HFF diet-induced MASH model. Mice fed NC diet (71.5% carbohydrates, 18.3% protein, and 10.2% fat) for 16 weeks served as controls.

Generation of Hepatic Knockout Mice

The CRISPR/Cas9 system was used to establish mice carrying a hepatocyte-specific *Otud5* deletion (*Otud5*-HKO) at the Animal Research Center of Nanjing University. $Otud5^{flox/flox}$ mice were then bred with albumin-Cre mice (Jackson Laboratory, Bar Harbor, ME) to establish *Otud5*-HKO mice; $Otud5^{flox/flox}$ (*Otud5*-Flox) mice served as controls.

Figure 12. (***See previous page***). **OTUD5 inhibits K48-linked ubiquitination and degradation of VDAC2.** (*A*) Left: expression levels of VDAC2 protein in HepG2 cells transfected with or without HA-OTUD5 plasmids. Cells were pretreated with 100 μg/mL CHX. Right: protein expression was normalized to that of β-actin. (*B*) Left: VDAC2 protein expression was determined in *OTUD5*-knockdown or control HepG2 cells; cells were pretreated with or without MG132 for 6 hours. Right: protein expression was normalized to that of β-actin. (*C*) Ubiquitination assays showing ubiquitination levels of endogenous VDAC2 in HepG2 cells with or without HA-OTUD5 transfection under PAOA treatment. (*D*) Ubiquitination assays showing ubiquitination levels of exogenous VDAC2 in HepG2 cells with HA-OTUD5 and Flag-VDAC2 plasmid transfection under PAOA treatment. (*E*) Ubiquitination assays displaying ubiquitination levels of endogenous VDAC2 in isolated primary hepatocytes from *Otud5*-HKO or *Otud5*-Flox mice under PAOA treatment. (*F*) Ubiquitination assays exhibiting ubiquitination of exogenous VDAC2 in HepG2 cells transfected with HA-OTUD5 or its mutant (C224S) plasmids, and Flag-VDAC2 plasmids under PAOA treatment. (*G*) Diverse forms of ubiquitin (K6O, K11O, K27O, K29O, K33O, K48O, and K63O) and Flag-VDAC2 were transfected into HepG2 cells with or without Flag-OTUD5. Cells were incubated with MG132 for 2 hours. Co-IP assays were then used. (*H*) Ubiquitination of Flag-VDAC2 after *OTUD5* overexpression was detected in HepG2 cells with wild-type (WT) or mutated Myc-Ub plasmid transfection under PAOA treatment. (*I*) Upper: the conserved K sites were marked in *yellow* (K23 and K31 in the N-terminal stretch of VDAC2). Lower: ubiquitination of Flag-VDAC2 or its mutants after *OTUD5* overexpression was determined in HepG2 cells with Myc-Ub plasmid transfection under PAOA treatment. (*J*) Upper: expression levels of Flag-VDAC2-2KR protein from HepG2 cells transfected with or without HA-OTUD5; cells were pretreated with MG132 for 6 hours. Lower: protein expression was standardized to β-actin. For all panels, data are presented as mean ± standard error of the mean (n = 3 independent experiments). *P* values were calculated by two-tailed unpaired Student *t* test. $^{**}P < .01$; ns, not significant.

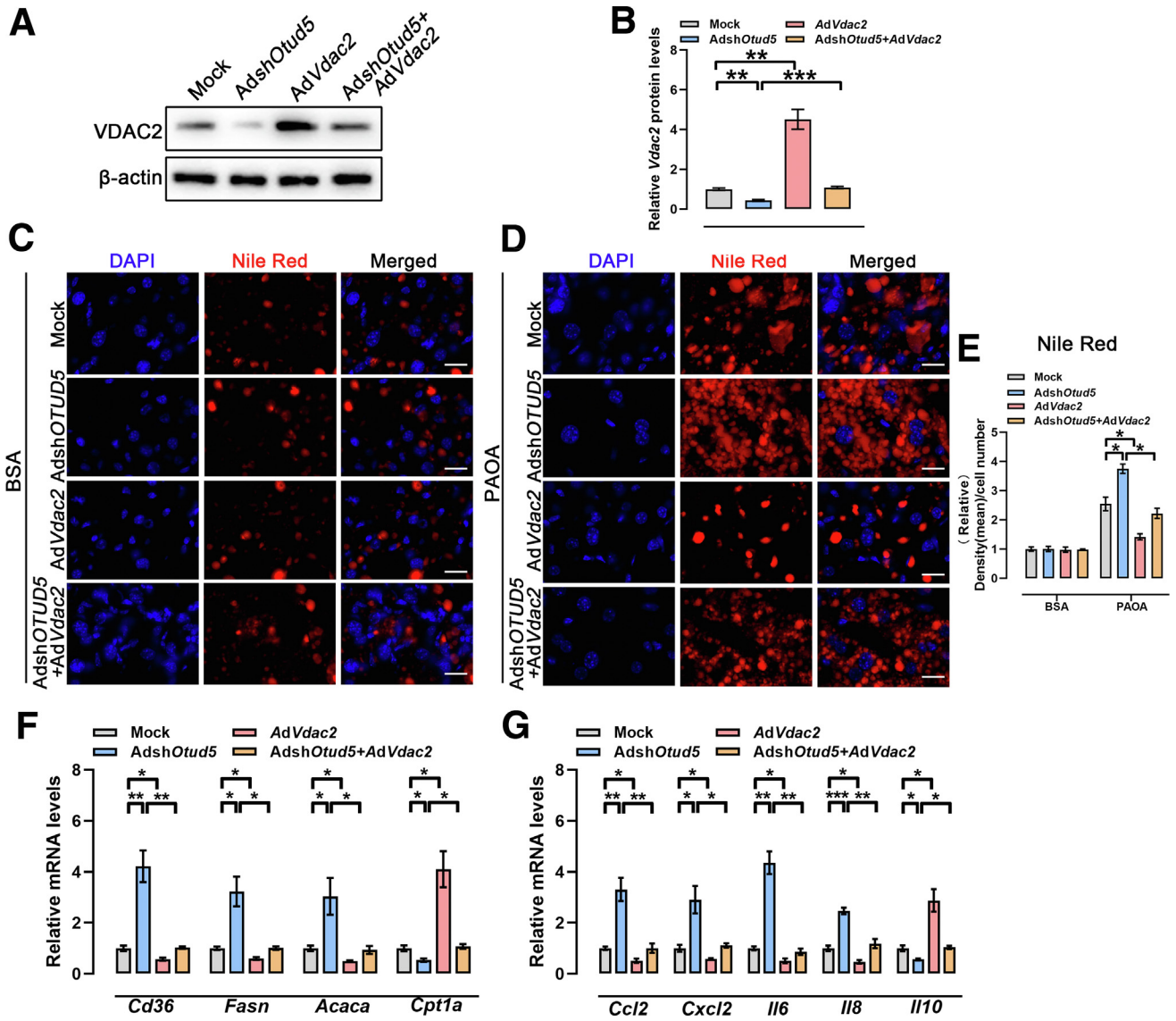

Figure 13. OTUD5 alleviates MASH by interacting with VDAC2. (*A* and *B*) Expression levels of VDAC2 protein in isolated primary hepatocytes infected with or without *OTUD5* knockdown or *VDAC2* overexpression. (*C* and *D*) Representative images of Nile Red staining in isolated primary hepatocytes infected with or without *OTUD5* knockdown or *VDAC2* overexpression under BSA/PAOA treatment. Scale bar: 25 μm. (*E*) Quantification of Nile Red staining density. (*F* and *G*) Relative mRNA expression levels of genes with respect to fatty acid metabolism (*F*) and inflammatory cytokines and chemokines (*G*) in primary hepatocytes transfected with or without *OTUD5* knockdown or *VDAC2* overexpression under PAOA treatment. For all panels, data are presented as mean ± standard error of the mean (n = 3 independent experiments). *P* values were calculated by two-tailed unpaired Student *t* test. **P* < .05; ***P* < .01; ****P* < .001.

Cell Lines

Human hepatoma cell line HepG2 and HEK293T were obtained from the Cell Bank of the Type Culture Collection of the Chinese Academy of Sciences. The cells were cultured in Dulbecco modified Eagle medium with 10% fetal bovine serum at 37°C in a humidified atmosphere with 5% CO_2.

Immunofluorescence Staining and Confocal Microscopy

For immunofluorescence staining, paraffin sections of liver tissues from humans and mice were incubated with primary antibodies overnight at 4°C and then labeled with fluorophore-conjugated secondary antibodies. Immunofluorescence images were captured using a fluorescence microscope. For confocal microscopy, cells transfected with HA-OTUD5 and Flag-VDAC2 were labeled with mouse anti-HA and rabbit anti-Flag-tag antibodies at 4°C and then incubated with fluorophore-conjugated secondary antibodies. Confocal images were acquired using a confocal laser scanning microscope.

qPCR Analysis

Total RNA from tissues and cells was extracted using the TRIzol reagent, and qPCR analysis was performed using the

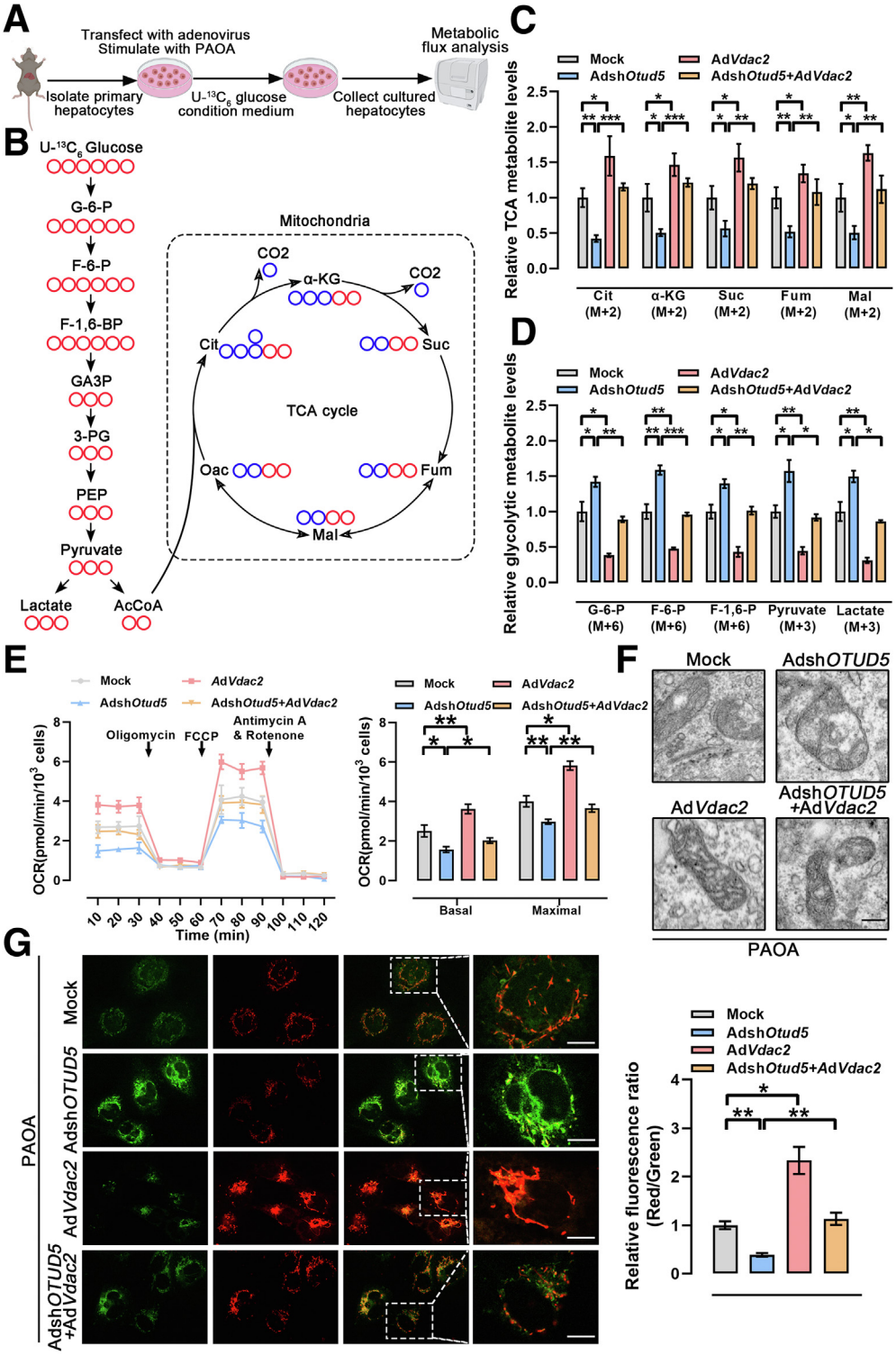

Figure 14. VDAC2 is indispensable in the role of OTUD5 on mitochondrial homeostasis. (*A* and *B*) Schema demonstrates intracellular fluxes in primary hepatocytes detected using U-$^{13}C_6$ glucose tracer. *Blue circle* indicates ^{12}C and *red circle* ^{13}C atoms. (*C* and *D*) Relative TCA metabolite levels (*C*) and relative glycolytic metabolite levels (*D*), as quantified by metabolic flux in primary mouse hepatocytes under PAOA treatment, with or without *OTUD5* knockdown or *VDAC2* overexpression. (*E*) Results of respiration detection in primary mouse hepatocytes under PAOA treatment, with or without *OTUD5* knockdown or *VDAC2* overexpression. (*F*) Representative pictures of mitochondrial morphology observed under transmission electron microscopy, with or without *OTUD5* knockdown or *VDAC2* overexpression (scale bar, 200 nm). (*G*) Representative images (left) and statistical results (right) of mitochondrial membrane potential visualization by JC-1 staining in primary mouse hepatocytes under PAOA treatment, with or without *OTUD5* knockdown or *VDAC2* overexpression. Scale bar: 10 μm. For all panels, data are presented as mean ± standard error of the mean (n = 3 independent experiments). *P* values were calculated by two-tailed unpaired Student *t* test. **P* < .05; ***P* < .01; ****P* < .001.

SYBR Green PCR Master Mix in Real-Time PCR System according to the manufacturer's instructions. Furthermore, mRNA expression levels were normalized to that of β-actin. The primers used are listed in Table 1.

Western Blot Analysis

Total protein from tissues and cells was isolated and lysed using RIPA lysis buffer and quantified using a BCA kit. The quantified proteins were separated using sodium dodecyl

sulfate-polyacrylamide gel electrophoresis and transferred to polyvinylidene difluoride membranes. The polyvinylidene difluoride membranes were blocked using 5% skimmed milk in tris-buffered saline tween, incubated with primary antibodies overnight at 4°C, and subsequently incubated with horseradish peroxidase–conjugated secondary antibodies. The indicated proteins were thereafter quantified using an electrochemoluminescent kit and a ChemiDoc MP Imaging System.

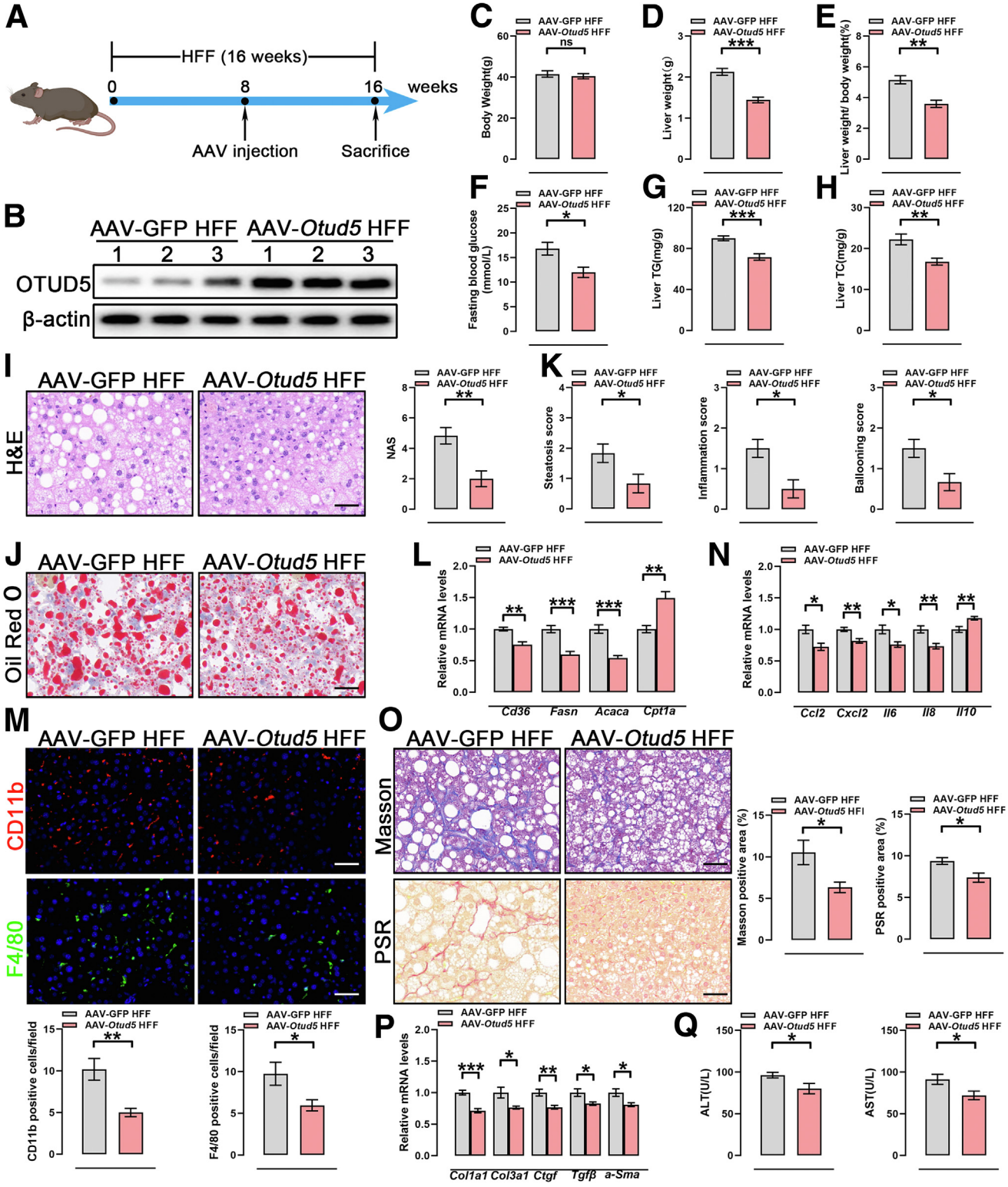

Primary Hepatocyte Isolation

To isolate primary hepatocytes from 6- to 8-week-old male C57BL/6 mice, collagenase perfusion and gradient centrifugation were performed as previously described.[48] A palmitic acid mixture (0.5 mmol/L; Sigma-Aldrich) and oleic acid (1.0 mmol/L; Sigma-Aldrich) was added to the medium for 12–16 hours to establish an in vitro model of lipid accumulation in hepatocytes.

Adenoviral Vector Construction

Three mouse adenovirus vector-mediated *OTUD5*-knockdown plasmids (Adsh*Otud5*), *OTUD5*-overexpression plasmids (Ad*Otud5*-Flag), and *VDAC2* overexpression plasmids (Ad*Vdac2*) were purchased from Haixing Biosciences (Suzhou, China). An adenovirus vector carrying *OTUD5* but lacking the OTU domain (Ad*OTUD5*-ΔOTU-Flag) was purchased from Haixing Biosciences. The shuttle plasmid pENTR-U6-CMV-flag-T2A-EGFP and ViraPower Adenoviral Expression System (V493-20; Invitrogen; Carlsbad, CA) were used to generate mouse *OTUD5*-overexpressing, *VDAC2*-overexpressing, or *OTUD5*-knockdown adenoviral vectors. The recombinant adenoviral vector was linearized by PacI (R0547L; New England Biolabs, Ipswich, MA) before co-transfection into 293 cells with polyethyleneimine (24765-1; Polysciences; Warrington, UK) transfection reagent. Cells were harvested after 6–7 days to assess the initial virus. The adenovirus was amplified by infecting 293 producer cells with the crude viral lysate, and the adenovirus was purified by cesium chloride density gradient centrifugation. Primary mouse hepatocytes were infected with adenovirus at a multiplicity of infection of 50.

Cellular Oil Red O Staining

Using 0.3% Oil Red O working solution, the HepG2 cells and primary mouse hepatocytes were stained for 30 minutes to detect intracellular lipid accumulation.

Cellular Nile Red Staining

HepG2 cells and primary mouse hepatocytes treated with BSA/PAOA were fixed in 4% paraformaldehyde. Subsequently, the cells were stained with Nile Red. Lipid accumulation was determined using a laser scanning confocal microscope.

Histopathologic Analysis

Paraffin-embedded and OCT-embedded liver sections from humans and mice were stained with H&E and Oil Red O, respectively. Liver fibrosis was determined using Masson's trichrome and Picrosirius red staining and visualized using a light microscope. The proportion of the Masson-positive and Picrosirius red–positive area was calculated using ImageJ software.

Mouse Metabolic and Liver Function Assays

Body weight and fasting serum blood glucose levels were monitored every 4 weeks. For glucose tolerance test assays, the mice were fasted for 6 hours, and their blood glucose levels were determined at the indicated time points after injection with 1 g/kg glucose or 0.75 IU/kg of insulin via the tail vein. Serum TG, TC, ALT, and AST levels were measured using an ADVIA 2400 Chemistry System Analyzer according to the manufacturer's instructions.

Immunoprecipitation Assays

IP assays were performed as previously described.[49] HepG2 and HEK293T cells transfected with the indicated plasmids were lysed using IP lysis buffer containing an inhibitor cocktail. After centrifugation, the samples were incubated overnight at 4°C with protein A/G agarose beads and the indicated anti-tag antibodies. For endogenous IP, cells were incubated with the primary antibody. The beads were then washed with IP lysis buffer. After centrifugation, the proteins were boiled in sodium dodecyl sulfate loading

Figure 15. (***See previous page***). **Hepatic *Otud5* overexpression by AAV alleviates HFF-induced MASH.** (*A*) Schematic showing injection of AAV-GFP or AAV-*Otud5* in HFF-fed mice. (*B*) Protein levels of OTUD5 in livers of HFF-fed mice after AAV-GFP or AAV-*Otud5* injection. n = 3 mice/group. (*C*) Body weights of HFF-fed mice after AAV-GFP or AAV-*Otud5* injection, respectively. n = 6 mice/group. (*D*) Liver weights of HFF-fed mice after AAV-GFP or AAV-*Otud5* injection, respectively. n = 6 mice/group. (*E*) Liver/body weight ratios of HFF-fed mice after AAV-GFP or AAV-*Otud5* injection, respectively. n = 6 mice/group. (*F*) Fasting blood glucose concentration of HFF-fed mice after AAV-GFP or AAV-*Otud5* injection, respectively. n = 6 mice/group. (*G* and *H*) Concentrations of hepatic TG (*G*) and TC (*H*) of HFF-fed mice after AAV-GFP or AAV-*Otud5* injection, respectively. n = 6 mice/group. (*I* and *J*) H&E (*I*) and Oil Red O (*J*) stained liver sections of HFF-fed mice after AAV-GFP or AAV-*Otud5* injection, respectively. NAS score was calculated. n = 6 mice/group. Scale bar: 50 μm. (*K*) Scores of hepatic steatosis, inflammation, and ballooning were quantified respectively. n = 6 mice/group. (*L*) Relative mRNA expression levels of genes with respect to fatty acid metabolism in livers of HFF-fed mice after AAV-GFP or AAV-*Otud5* injection, respectively. n = 6 mice/group. (*M*) Immunofluorescence images of CD11b (*red*) and F4/80 (*green*) in livers of HFF-fed mice after AAV-GFP or AAV-*Otud5* injection, respectively. Percentages of $CD11b^+$ and $F4/80^+$ cells were quantified. n = 6 mice/group. Scale bar: 50 μm. (*N*) Relative mRNA expression levels of genes related to inflammation in livers of HFF-fed mice after AAV-GFP or AAV-*Otud5* injection, respectively. n = 6 mice/group. (*O*) Left: Masson (upper) and PSR (lower) stained livers of HFF-fed mice after AAV-GFP or AAV-*Otud5* injection, respectively. n = 6 mice/group. Scale bar: 50 μm. Right: quantification of Masson and PSR positive cells. (*P*) Relative mRNA expression levels of genes related to fibrosis in livers of HFF-fed mice after AAV-GFP or AAV-*Otud5* injection, respectively. n = 6 mice/group. (*Q*) Serum ALT and AST concentrations of HFF-fed mice after AAV-GFP or AAV-*Otud5* injection, respectively. n = 6 mice/group. For all panels, data are presented as mean ± standard error of the mean, and n represents biologically independent repeats. *P* values were calculated by two-tailed unpaired Student *t* test. $^*P < .05$; $^{**}P < .01$; $^{***}P < .001$; ns, not significant.

Table 1. Primers Sequences Used for Real-Time PCR

Gene	Species	Sequence (5′-3′)
OTUD1	Human	Forward: GACGAGAAGCTGGCCCTATAC Reverse: TGGAATGATGTGGAATCGGTACT
OTUD2	Human	Forward: ATGTTTGGCCCCGCTAAAGG Reverse: CGGTGATGGCGGCAATTTG
OTUD3	Human	Forward: TGCGAGGAGGAGTTCGTCA Reverse: GTGCTTGAGATGATTTCGTGAGT
OTUD4	Human	Forward: TTCTGATGTGGATTACAGAGGGC Reverse: ACGCATGTTGTCTTACTCCTGA
OTUD5	Human	Forward: GGTTGTGCGAAAGCATTGCAT Reverse: ACCTCCACAGGACGGTTGT
OTUD6A	Human	Forward: ATGGATGATCCGAAGAGTGAACA Reverse: GGTCTTGGGGACCGAGTTTT
OTUD6B	Human	Forward: TGAGAAGGCATCGCAAAGAGA Reverse: ATCTTCGGTGAGTTGCTTCCT
ALG13	Human	Forward: AAGTGCGTGTTTGTTACCGTA Reverse: ATTTGCAGGATAAGTCGGTTGT
Otud1	Mouse	Forward: AGAGGCAGGACAAGTACCTGA Reverse: CCCGTACACAGTCTTGCTGAC
Otud2	Mouse	Forward: TCAGCGAATCCTCGTTGGC Reverse: GCATGTCACCTGACTGGATGG
Otud3	Mouse	Forward: GAGCTTCGCCAACCAACTG Reverse: CGCTGCCTTATCATGTAGTCC
Otud4	Mouse	Forward: GCAAACTGGGCTTGTATCGGA Reverse: CACATGCCGAGACTGAGAGTG
Otud5	Mouse	Forward: AACAGTGAAGACGAGTATGAAGC Reverse: GCCTTTTCAAACCAGTGTTCCTG
Otud6A	Mouse	Forward: GAACTCCAACGGGTGATCCG Reverse: CTTGTCGTTCTTTGGGACGG
Otud6B	Mouse	Forward: AACGCTGTTCCCAAAAACGAC Reverse: GGTGGTTGATTCTCAAGTACCAA
Alg13	Mouse	Forward: AAGAGAGCGTTTGTGACTGTC Reverse: GGAATGGTTTGGGCACCAC
Cd36	Mouse	Forward: ATGGGCTGTGATCGGAACTG Reverse: TTTGCCACGTCATCTGGGTTT
Fasn	Mouse	Forward: GGAGGTGGTGATAGCCGGTAT Reverse: TGGGTAATCCATAGAGCCCAG
Acaca	Mouse	Forward: CTCCCGATTCATAATTGGGTCTG Reverse: TCGACCTTGTTTTACTAGGTGC
Cpt1a	Mouse	Forward: TGGCATCATCACTGGTGTGTT Reverse: GTCTAGGGTCCGATTGATCTTTG
Ccl2	Mouse	Forward: TAAAAACCTGGATCGGAACCAAA Reverse: GCATTAGCTTCAGATTTACGGGT
Cxcl2	Mouse	Forward: CCAACCACCAGGCTACAGG Reverse: GCGTCACACTCAAGCTCTG
Il6	Mouse	Forward: CTGCAAGAGACTTCCATCCAG Reverse: AGTGGTATAGACAGGTCTGTTGG
Il8	Mouse	Forward: TCGAGACCATTTACTGCAACAG Reverse: CATTGCCGGTGGAAATTCCTT
Il10	Mouse	Forward: CTTACTGACTGGCATGAGGATCA Reverse: GCAGCTCTAGGAGCATGTGG
Col1a1	Mouse	Forward: GCTCCTCTTAGGGGCCACT Reverse: ATTGGGGACCCTTAGGCCAT
Col3a1	Mouse	Forward: CTGTAACATGGAAACTGGGGAAA Reverse: CCATAGCTGAACTGAAAACCACC
Ctgf	Mouse	Forward: GGCCTCTTCTGCGATTTCG Reverse: GCAGCTTGACCCTTCTCGG
Tgfβ	Mouse	Forward: CCACCTGCAAGACCATCGAC Reverse: CTGGCGAGCCTTAGTTTGGAC
α-Sma	Mouse	Forward: CCCAGACATCAGGGAGTAATGG Reverse: TCTATCGGATACTTCAGCGTCA
TNF	Human	Forward: CCTCTCTCTAATCAGCCCTCTG Reverse: GAGGACCTGGGAGTAGATGAG
IL6	Human	Forward: ACTCACCTCTTCAGAACGAATTG Reverse: CCATCTTTGGAAGGTTCAGGTTG

buffer for 10 minutes. Finally, Western blotting analysis was performed.

Mass Spectrometry Analysis

As described in IP assays, OTUD5 and its interacting proteins were immunoprecipitated. Proteins were subjected to liquid chromatography coupled to tandem mass spectrometry analysis.

Ubiquitination Assays

Hepatocytes transfected with the various plasmids were boiled in sodium dodecyl sulfate loading buffer for 10 minutes. Subsequently, the lysates were treated with 0.9 mL IP lysis buffer. After sonication and centrifugation, the supernatants were incubated with anti-tag or antibodies of the target proteins and protein A/G agarose beads at 4°C. The beads were then rinsed twice with IP lysis buffer. After centrifugation, sodium dodecyl sulfate loading buffer was added to the protein, and the mixture was boiled for 10 minutes. Western blotting analysis was performed.

Statistical Analysis

Statistical analyses were performed using the GraphPad Prism version 9. Means between 2 groups were analyzed using Student t test (unpaired two-tailed). Pearson's correlation analysis was used to determine the correlations between the 2 variables. Statistical significance was set at $P < .05$.

References

1. Li X, Ding K, Li X, et al. Deficiency of WTAP in hepatocytes induces lipoatrophy and non-alcoholic steatohepatitis (NASH). Nature Communications 2022;13:4549.
2. Gao H, Jin Z, Bandyopadhyay G, et al. Aberrant iron distribution via hepatocyte-stellate cell axis drives liver lipogenesis and fibrosis. Cell Metabolism 2022; 34:1201–1213 e5.
3. Allen AM, Therneau TM, Ahmed OT, et al. Clinical course of non-alcoholic fatty liver disease and the implications for clinical trial design. J Hepatol 2022; 77:1237–1245.
4. Qiu H, Song E, Hu Y, et al. Hepatocyte-secreted autotaxin exacerbates nonalcoholic fatty liver disease through autocrine inhibition of the PPARα/FGF21 axis. Cell Mol Gastroenterol Hepatol 2022;14:1003–1023.

5. Huang X, Yao Y, Hou X, et al. Macrophage SCAP contributes to metaflammation and lean NAFLD by activating STING-NF-κB signaling pathway. Cell Mol Gastroenterol Hepatol 2022;14:1–26.
6. Chang D, Truong E, Mena EA, et al. Machine learning models are superior to noninvasive tests in identifying clinically significant stages of NAFLD and NAFLD-related cirrhosis. Hepatology 2023;77:546–557.
7. Riazi K, Azhari H, Charette JH, et al. The prevalence and incidence of NAFLD worldwide: a systematic review and meta-analysis. Lancet Gastroenterol Hepatol 2022; 7:851–861.
8. Chen XW, Ding G, Xu L, et al. A glimpse at the metabolic research in China. Cell Metab 2021;33:2122–2125.
9. Lekka E, Kokanovic A, Mosole S, et al. Pharmacological inhibition of Lin28 promotes ketogenesis and restores lipid homeostasis in models of non-alcoholic fatty liver disease. Nat Commun 2022;13:7940.
10. Ling Y, Li Y, Li L. Targeting folliculin to selectively inhibit mTORC1: a promising strategy for treating nonalcoholic fatty liver disease. Signal Transduct Target Ther 2022; 7:277.
11. Huang DQ, Singal AG, Kono Y, et al. Changing global epidemiology of liver cancer from 2010 to 2019: NASH is the fastest growing cause of liver cancer. Cell Metab 2022;34:969–977 e2.
12. Zhang P, Chen Z, Kuang H, et al. Neuregulin 4 suppresses NASH-HCC development by restraining tumor-prone liver microenvironment. Cell Metab 2022;34:1359–1376 e7.
13. Ge C, Tan J, Dai X, et al. Hepatocyte phosphatase DUSP22 mitigates NASH-HCC progression by targeting FAK. Nat Commun 2022;13:5945.
14. Peng Y, Wong CC, Yu J. The paradox of immunotherapy in NASH-HCC. Signal Transduct Target Ther 2021;6:228.
15. Wang F, Zhang X, Liu W, et al. Activated natural killer cell promotes nonalcoholic steatohepatitis through mediating JAK/STAT pathway. Cell Mol Gastroenterol Hepatol 2022;13:257–274.
16. Peiseler M, Schwabe R, Hampe J, et al. Immune mechanisms linking metabolic injury to inflammation and fibrosis in fatty liver disease: novel insights into cellular communication circuits. J Hepatol 2022;77:1136–1160.
17. Shah PA, Patil R, Harrison SA. NAFLD-related hepatocellular carcinoma: the growing challenge. Hepatology 2023;77:323–338.
18. Xu X, Poulsen KL, Wu L, et al. Targeted therapeutics and novel signaling pathways in non-alcohol-associated fatty liver/steatohepatitis (NAFL/NASH). Signal Transduct Target Ther 2022;7:287.
19. Gines P, Castera L, Lammert F, et al. Population screening for liver fibrosis: toward early diagnosis and intervention for chronic liver diseases. Hepatology 2022; 75:219–228.
20. Hong CH, Ko MS, Kim JH, et al. Sphingosine 1-phosphate receptor 4 promotes nonalcoholic steatohepatitis by activating NLRP3 inflammasome. Cell Mol Gastroenterol Hepatol 2022;13:925–947.
21. Truongvan N, Li S, Misra M, et al. Structures of UBA6 explain its dual specificity for ubiquitin and FAT10. Nature Communications 2022;13:4789.
22. Li Q, Zhang L, You W, et al. PRDM1/BLIMP1 induces cancer immune evasion by modulating the USP22-SPI1-PD-L1 axis in hepatocellular carcinoma cells. Nat Commun 2022;13:7677.
23. Cai C, Tang YD, Zhai J, et al. The RING finger protein family in health and disease. Signal Transduct Target Ther 2022;7:300.
24. Wang F, Zhang Y, Shen J, et al. The ubiquitin E3 ligase TRIM21 promotes hepatocarcinogenesis by suppressing the p62-Keap1-Nrf2 antioxidant pathway. Cell Mol Gastroenterol Hepatol 2021;11:1369–1385.
25. Jenkin KA, Han Y, Lin S, et al. Nedd4-2-dependent ubiquitination potentiates the inhibition of human NHE3 by cholera toxin and enteropathogenic Escherichia coli. Cell Mol Gastroenterol Hepatol 2022;13:695–716.
26. Xu MX, Tan J, Ge CX, et al. Tripartite motif-containing protein 31 confers protection against nonalcoholic steatohepatitis by deactivating mitogen-activated protein kinase kinase kinase 7. Hepatology 2023; 77:124–143.
27. Yang Q, Chen X, Zhang Y, et al. The E3 ubiquitin ligase Ring finger protein 5 ameliorates NASH through ubiquitin-mediated degradation of 3-hydroxy-3-methylglutaryl CoA reductase degradation protein 1. Hepatology 2021;74:3018–3036.
28. Wang L, Zhang X, Lin ZB, et al. Tripartite motif 16 ameliorates nonalcoholic steatohepatitis by promoting the degradation of phospho-TAK1. Cell Metab 2021; 33:1372–1388 e7.
29. Kwasna D, Abdul Rehman SA, Natarajan J, et al. Discovery and characterization of ZUFSP/ZUP1, a distinct deubiquitinase class important for genome stability. Molecular Cell 2018;70:150–164 e6.
30. Zhu Q, Fu Y, Li L, et al. The functions and regulation of Otubains in protein homeostasis and diseases. Ageing Res Rev 2021;67:101303.
31. Liu W, Yan B, Yu H, et al. OTUD1 stabilizes PTEN to inhibit the PI3K/AKT and TNF-alpha/NF-kappaB signaling pathways and sensitize ccRCC to TKIs. Int J Biol Sci 2022;18:1401–1414.
32. Zhou N, Qi H, Liu J, et al. Deubiquitinase OTUD3 regulates metabolism homeostasis in response to nutritional stresses. Cell Metab 2022;34:1023–1041 e8.
33. Kayagaki N, Phung Q, Chan S, et al. DUBA: a deubiquitinase that regulates type I interferon production. Science 2007;318:1628–1632.
34. Rutz S, Kayagaki N, Phung QT, et al. Deubiquitinase DUBA is a post-translational brake on interleukin-17 production in T cells. Nature 2015;518:417–421.
35. Dinallo V, Di Fusco D, Di Grazia A, et al. The deubiquitinating enzyme OTUD5 sustains inflammatory cytokine response in inflammatory bowel disease. J Crohns Colitis 2022;16:122–132.
36. Kang XY, Zhang J, Tang L, et al. OTU deubiquitinase 5 inhibits the progression of non-small cell lung cancer via regulating p53 and PDCD5. Chem Biol Drug Des 2020; 96:790–800.
37. Yin F, He H, Zhang B, et al. Effect of deubiquitinase ovarian tumor domain-containing protein 5 (OTUD5) on radiosensitivity of cervical cancer by regulating the

ubiquitination of Akt and its mechanism. Med Sci Monit 2019;25:3469–3475.
38. Zhang Y, Fan Y, Jing X, et al. OTUD5-mediated deubiquitination of YAP in macrophage promotes M2 phenotype polarization and favors triple-negative breast cancer progression. Cancer Lett 2021;504:104–115.
39. Hou T, Dan W, Liu T, et al. Deubiquitinase OTUD5 modulates mTORC1 signaling to promote bladder cancer progression. Cell Death Dis 2022;13:778.
40. Liu D, Zhang P, Zhou J, et al. TNFAIP3 interacting protein 3 overexpression suppresses nonalcoholic steatohepatitis by blocking TAK1 activation. Cell Metab 2020;31:726–740.e8.
41. Yang Y, Luo M, Zhang K, et al. Nedd4 ubiquitylates VDAC2/3 to suppress erastin-induced ferroptosis in melanoma. Nat Commun 2020;11:433.
42. Fu J, Hu F, Ma T, et al. A conventional immune regulator mitochondrial antiviral signaling protein blocks hepatic steatosis by maintaining mitochondrial homeostasis. Hepatology 2022;75:403–418.
43. Diaz LA, Fuentes-Lopez E, Ayares G, et al. The establishment of public health policies and the burden of nonalcoholic fatty liver disease in the Americas. Lancet Gastroenterol Hepatol 2022;7:552–559.
44. Ginsberg HN, Mani A. Complex regulation of fatty liver disease. Science 2022;376:247–248.
45. van Delft MF, Chappaz S, Khakham Y, et al. A small molecule interacts with VDAC2 to block mouse BAK-driven apoptosis. Nature Chemical Biology 2019;15:1057–1066.
46. Roy SS, Ehrlich AM, Craigen WJ, et al. VDAC2 is required for truncated BID-induced mitochondrial apoptosis by recruiting BAK to the mitochondria. EMBO Reports 2009;10:1341–1347.
47. Kleiner DE, Brunt EM, Van Natta M, et al. Design and validation of a histological scoring system for nonalcoholic fatty liver disease. Hepatology 2005;41:1313–1321.
48. Sun N, Shen C, Zhang L, et al. Hepatic Kruppel-like factor 16 (KLF16) targets PPARalpha to improve steatohepatitis and insulin resistance. Gut 2021;70:2183–2195.
49. Li Q, Ni Y, Zhang L, et al. HIF-1alpha-induced expression of m6A reader YTHDF1 drives hypoxia-induced autophagy and malignancy of hepatocellular carcinoma by promoting ATG2A and ATG14 translation. Signal Transduction and Targeted Therapy 2021;6:76.

Received August 12, 2023. Accepted November 27, 2023.

Correspondence
Address correspondence to: Qing Li, PhD, MD, Jiangsu Province Hospital and Nanjing Medical University, First Affiliated Hospital, Guangzhou Road 300, Nanjing, 210029, China. e-mail: liqingjsph@njmu.edu.cn; or Jun Li, PhD, MD, Jiangsu Province Hospital and Nanjing Medical University, First Affiliated Hospital, Guangzhou Road 300, Nanjing, 210029, China. e-mail: drlijun@vip.sina.com; or Xinzheng Dai, PhD, MD, Jiangsu Province Hospital and Nanjing Medical University, First Affiliated Hospital, Guangzhou Road 300, Nanjing, 210029, China. e-mail: daixinzheng@njmu.edu.cn; or Ke Jin, PhD, MD, Jiangsu Province Hospital and Nanjing Medical University, First Affiliated Hospital, Guangzhou Road 300, Nanjing, 210029, China. e-mail: penghaoren2001@126.com; or Longfeng Jiang, PhD, MD, Jiangsu Province Hospital and Nanjing Medical University, First Affiliated Hospital, Guangzhou Road 300, Nanjing, 210029, China. e-mail: longfengjiang@njmu.edu.cn; or Jingjing Dai, MD, Jiangsu Province Hospital and Nanjing Medical University, First Affiliated Hospital, Guangzhou Road 300, Nanjing, 210029, China. e-mail: 15951088290@163.com.

CRediT Authorship Contributions
Jingjing Dai (Conceptualization: Equal; Data curation: Lead; Project administration: Lead)
Liren Zhang (Methodology: Lead; Supervision: Lead; Visualization: Equal)
Ruizhi Zhang (Resources: Supporting; Software: Equal; Visualization: Lead; Writing – review & editing: Equal)
Jing Ge (Data curation: Lead; Software: Lead; Validation: Lead)
Feifan Yao (Investigation: Lead; Methodology: Supporting; Project administration: Equal)
Suiqing Zhou (Formal analysis: Equal; Investigation: Equal; Supervision: Equal; Writing – original draft: Supporting)
Jiali Xu (Conceptualization: Supporting; Data curation: Equal; Investigation: Supporting; Resources: Lead)
Kai Yu (Software: Supporting)
Jing Xu (Formal analysis: Lead; Software: Lead)
Longfeng Jiang (Conceptualization: Supporting; Investigation: Lead; Resources: Lead; Supervision: Lead)
Ke Jin (Methodology: Lead; Resources: Lead; Supervision: Lead)
Xinzheng Dai (Funding acquisition: Equal; Resources: Equal; Software: Supporting)
Jun Li (Data curation: Lead; Funding acquisition: Lead; Investigation: Lead; Resources: Lead)
Qing Li (Conceptualization: Lead; Funding acquisition: Lead; Methodology: Lead)

Conflicts of interest
The authors disclose no conflicts.

Funding
Supported by the National Natural Science Foundation of China (82203659 and 82103440) and the Natural Science Foundation of Jiangsu Province (BK20220731).